Post-depositional evolution over a time scale of 1 million years of eastern Mediterranean organic-rich and organic-poor sediments: new insights on the debromination and layer-silicate markers

Anne Murat, Daniel Beaufort, Benoît Hebert, François Baudin, Stefano Bernasconi, Emmanuelle Ducassou, Céline Lelievre, Emmanuel Poizot, Maximilien Mathian, O. Grauby

Post-depositional evolution over a time scale of 1 million years of eastern Mediterranean organic-rich and organic-poor sediments: new insights on the debromination and layer-silicate markers

Evolution post-dépôt à l'échelle d'un million d'années de sédiments riches et pauvres en matière organique en Méditerranée orientale: nouveaux aperçus sur la débromination et les marqueurs argileux

Anne MURAT[(1,2)], Daniel BEAUFORT[(3)], Benoît HEBERT[(3)], François BAUDIN[(4)], Stefano BERNASCONI[(5)], Emmanuelle DUCASSOU[(6)], Céline LELIEVRE[(1)], Emmanuel POIZOT[(1,2)], Maximilien MATHIAN[(3)] and Olivier GRAUBY[(7)]

(1) Laboratoire universitaire des sciences appliquées de Cherbourg. Normandie Univ., UNICAEN, LUSAC, 50100 Cherbourg, France

(2) Conservatoire National des Arts et Métiers. INTECHMER, 50100 Cherbourg, France

(3) IC2MP UMR 7285, Université de Poitiers, 86073 Poitiers cedex 9, France

(4) iSTeP, UMR 7193, Université de Paris VI, 75005 Paris, France

(5) Geologisches Institut, ETHZ Zuerich, 8092 Zuerich, Switzerland

(6) UMR-CNRS 5805 EPOC, Université de Bordeaux, 33615 Pessac cedex, France

(7) UMR 7325 CINaM/CNRS, Université Aix-Marseille campus de Luminy, 13288 Marseille cedex 9, France

Email: anne.murat@cnam.fr

Key words: organic matter, clay minerals, bromine, eogenesis, sapropel, Mediterranean sea

Mots clés : matière organique, minéraux argileux, brome, éogenèse, sapropèle, mer Méditerranée

Abstract

Organic matter degradation is the engine behind the biogeochemical evolution of sediments during burial. Previous research has shown that eogenesis is the seat of a complex interplay between organic matter, microbes and the most reactive part of inorganic compounds, such as clay minerals. To explore the variability and stability of bromine and clay minerals as geochemical and mineral tracers, we selected an eastern Mediterranean core that has a high degree of stability in the quality and quantity of organic matter through time at a one-million-year scale and great variability in organic matter content at a 10 ky scale. According to the very low maximal burial depth reached by these sediments (the core length is only 36.5 m), physical parameters, such as temperature and pressure, did not significantly influence the evolution of the studied parameters during the burial history. The bulk clay mineralogy of organic-rich and organic-poor sediments is similar all along the investigated core material; smectite predominates over kaolinite. The only identified authigenic minerals are biogenetic framboidal pyrite and manganese oxides. The X-ray data and the chemical compositions of the smectite are characteristic of a montmorillonite which is representative of a detrital Nile source. At a one-million-year scale, the organic matter content has no significant influence on clay eogenesis, and detrital smectite and kaolinite remain unchanged. Bromine is present in marine organic matter as organobromine compounds. During eogenesis, bromine is released from organic matter as bromide ion, resulting in an increase in the bromide concentration in the pore water with depth. Dissolved bromide can be used as a

conservative tracer of the debromination of sedimentary organic matter. For the first time, we established that solid-phase BrOrg is a reliable tracer of debromination rates in marine sediments. The rate of debromination depends on the organic matter content. The rate increases from less than 2.3 x 10^{-4} µmolBrOrg $molC^{-1}$ y^{-1} to 6.3 x 10^{-4} µmolBrOrg $molC^{-1}$ y^{-1} when TOC varies from 0.17 to 3%. This increase is related to the development of the bacterial population and provides the basis for further investigation of other oceanic basins. For TOC values >4%, the rate of debromination decreases. We propose that the bioavailability of organic matter is another factor of variability in the debromination rate.

Résumé

La dégradation de la matière organique est le moteur de l'évolution biogéochimique des sédiments au cours de l'enfouissement. Les recherches précédentes ont montré que l'éogenèse est le siège d'interférences complexes entre la matière organique, les microorganismes et la partie la plus réactive des composés inorganiques comme les minéraux argileux. Pour étudier la variabilité et la stabilité de traceurs géochimiques et minéralogiques, le brome et les minéraux argileux, nous avons choisi une carotte de Méditerranée orientale qui présente une grande stabilité de la qualité et de la quantité de la matière organique à l'échelle de 1 million d'années et une grande variabilité de cette quantité à une échelle de 10 ka. Considérant le faible enfouissement de ces dépôts (la carotte ne fait que 36,5 m de long), les paramètres physiques comme la température et la pression, n'influencent pas significativement l'évolution des paramètres étudiés. La minéralogie des argiles demeure semblable dans toute la carotte, que les sédiments soient riches ou pauvres en matière organique ; la smectite domine sur la kaolinite. Les seuls minéraux authigéniques identifiés sont la pyrite framboïdale biogénique et des oxydes de manganèse. Les

75 données de diffraction de rayons X et la composition chimique de la smectite
76 correspondent à celles d'une montmorillonite représentative des apports détritiques
77 du Nil. A l'échelle de 1 million d'années, la quantité de matière organique n'influence
78 pas l'éogenèse des minéraux argileux, la kaolinite et la smectite détritique demeurent
79 inchangées. Le brome est dans la matière organique marine sous forme de
80 composés organobromés. Pendant l'éogenèse, le brome est libéré de la matière
81 organique sous forme d'ion bromure, il en résulte une augmentation avec
82 l'enfouissement de la concentration en bromure dans l'eau interstitielle. Le bromure
83 dissous peut être utilisé comme un traceur conservatif de la débromination de la
84 matière organique sédimentaire. Pour la première fois, nous avons établi que le
85 brome organique particulaire est un traceur valide du taux de débromination dans les
86 sédiments marins. Le taux de débromination dépend de la quantité de matière
87 organique. Il augmente de 2.3 x 10^{-4} µmolBrOrg molC^{-1} y^{-1} à 6.3 x 10^{-4} µmolBrOrg
88 molC^{-1} y^{-1} quand le Carbone Organique Total (COT) varie de 0.17 à 3%. Cette
89 augmentation est en relation avec le développement des populations bactériennes et
90 fournit une base pour l'étude d'autres bassins océaniques. Pour les teneurs en COT
91 >4%, le taux de débromination diminue. Nous proposons que la biodisponibilité de la
92 matière organique soit un autre facteur de variabilité du taux de débromination.

93 1 Introduction

94 The early evolution of sediments is an important gap in the fundamental
95 understanding of the eogenetic processes during the very shallow burial of both
96 organic and inorganic matter [Barnes et al., 1990; McKinley et al., 2003; Worden and
97 Morad, 2003; Worden and Burley, 2003]. The term eogenesis covers the very
98 shallow diagenesis of both organic and inorganic matter. Eogenetic mineral reactions
99 include the interaction of detrital mineral assemblages with pore water under the

influence of a depositional system (Burley, 1993). Such reactions proceed at low temperature and are partly biochemical because they occur most often in the bacterial sulfate reduction zone (Barnes et al., 1990, Surdam et al. 1989).Organic matter degradation is the engine behind the biogeochemical evolution of sediments during burial. Field observations primarily target shallow sediment depths and fast-decaying materials, although organic matter, particularly the most refractory compounds, may degrade on geological timescales [Middelburg, 1989; Arndt et al., 2013]. Previous research showed that eogenesis is the seat of a complex interplay between organic matter, microbes and the most reactive part of the inorganic compounds, such as clay minerals. It has been established that organic matter stabilization occurs through the formation of organo-mineral complexes with layer-silicates, such as expandable clays, which are responsible for the reduction in the bioavailability of organic molecules [Mayer, 1994]. Organic matter and bacteria are known to influence the earliest reaction of non-silicates (sulfides, carbonates) and are suspected to have a role during clay eogenesis [Pryor, 1975; Coleman, 1985; Worden and Morad, 2003]. Moreover, because eogenesis is influenced by the residence time of the pore fluids, the early diagenetic assemblages are also governed by the control of sedimentation, such as climate, the rate of subsidence and the rate of sedimentation [Worden and Burley, 2003].

The aim of this study is to highlight both the organic matter and layer silicates evolution during eogenesis based on the variability or stability of bromine and clay mineral geochemical tracers.

Inorganic bromine is found as soluble bromine salts in seawater, but there are also numerous (200) known organobromine compounds that are synthesized by living organisms or formed during natural abiotic processes, such as forest fires or volcanic

eruption [Gribble, 2003]. Bromine is present in marine organic matter as organobromine compounds, and a direct correlation between the bromine content and organic carbon content of sediments has been found by several authors [Price and Calvert, 1977; Pedersen and Price, 1980; Ten Haven et al., 1988; Martin et al., 1993; Ziegler et al., 2008; Leri et al. 2010]. During eogenesis, bromine is released from organic matter as bromide ion, resulting in an increase in the bromide concentration in pore water with depth [Gieskes and Mahn, 2007]. Dissolved bromide can be used as a conservative tracer of the debromination of sedimentary organic matter [Upstill-Goddard and Elderfield, 1988; Mahn and Gieskes, 2001; Berg and Solomon, 2016]. It is generally accepted that the variations in the source of organic matter, supply rate and initial solid-phase bromine concentration make the solid-phase bromine concentration an unreliable tracer for debromination in marine sediments [Berg and Solomon, 2016]. We assume that it is possible to calculate the debromination rate based on the solid-phase bromine concentration variability through time.

To achieve this objective and to explore clay mineral evolution, the studied sediment must satisfy certain requirements. The investigated site must display a high degree of stability through time of: (1) the sediment supply characteristics, (2) the sedimentation rate, which must be moderate to provide limited burial, and (3) the quality and quantity of the organic supply at one-million-year scale. However, to investigate the effect of the total organic carbon (TOC) concentration on debromination and clay mineral evolution, large variability in the organic matter content is required at a 10 ky scale.

The sediments of the eastern Mediterranean sea are good candidates to explore the evolution of organic matter during burial and over time. Organic-poor and organic-rich

(sapropels) layers occur periodically in the sedimentary sequences due to a recurrent decline in deep-water ventilation. Sapropels have been the subject of many publications since the 1970s; Meyers [2006] and Rohling et al. [2015] are two of the most recent studies. This study focuses on the Neogene sediments of the Nile margin, which are situated in the far eastern Mediterranean sea, a location that enhances the sapropel layer registration in a smectite-rich sedimentary column.

2 Material and methods

2-1 Material

Core MD04 2723 (latitude 32°59.99'N, longitude 33°08.01'E, 1527 m water depth, 36.54 m long) was collected on the eastern part of the Nile continental margin during the Vanil cruise of Marion Dufresne II in 2004 (Fig. 1). This margin was built by the Nile river, one of the longest rivers in the world with a summer flood regime. Several high magnitude flood periods occurred during the Quaternary, which have been correlated with the periodic intensification of monsoonal activity over the Nile headwaters [Hassan, 1981; Rossignol-Strick, 1985; Emeis et al., 2000; Kallel et al., 2000; Schilman et al., 2001]. Nile floods and/or enhanced rainfall over the basin represent significant potential sources of fresh water for the Levantine basin. This fresh water increased the density stratification of the water column and organic matter preservation, and nutrients brought in by the runoff enhanced productivity. These conditions can trigger sapropel deposition [Olausson, 1961; Rohling, 1994; Béthoux and Pierre, 1999; Cramp and O'Sullivan, 1999; Jorissen, 1999; Casford et al., 2003; Meyers, 2006; Rohling et al., 2015]. Sapropels are episodic, basin-wide organic-rich layers that characterize the Neogene sedimentary sequences of the Mediterranean Sea. The classic lithostratigraphy of the eastern Mediterranean is

based on isochronous sapropel deposits, which are synchronous throughout the deep-water basins [Kroon et al., 1998; Kallel et al., 2000; Ducassou et al., 2007]. Sapropels were identified in the studied core based on the lithological characteristics and total organic carbon (TOC) content. They appear as dark greenish and oily layers, laminated or bioturbated depending on their thickness; homogenous, color-banded or composite; with a TOC of at least 1% [Murat and Got, 2000]. The studied core has a continuous and undisturbed sedimentary record of sapropelic sequences numbered from 1 for the youngest to 29 for the oldest according to the usual standard.

2-2 Methodology

2-2-1 Sampling strategy

Core scanner measurements were conducted on a slab collected at the surface of the archive half core. The slabs were then regularly sampled to obtain isotopic data.

Geochemical analysis (TOC, Ca and Br) and characterization of clay minerals were performed on samples from the work half core. We considered 18 sapropelic sequences of the available 28 (S1, S3, S5, S6, S7, S9, S10, S11, S12, S15, S17, S19, S21, S23, S24, S27, S28 and S29) to obtain regular information through time and conducted high-frequency sampling. “Sapropelic sequence” refers to a set of samples collected below, inside and above the sapropel itself. Each sapropelic sequence corresponds to a sedimentation period ranging from 10 to 20 ky. We added a series of non-sapropelic samples deposited between 17 and 60 ka during isotopic stages 2 to 4.

To match the data obtained from the archive slab and work half core, lithologic description was performed for both. The final lithologic synthesis was based on the

198 archive slab half core depths. The depths of the work half core samples were
199 recalculated when necessary.

200 2-2-2 Isotope analysis

201 Stable isotope measurements were carried out every 10 cm. Samples were dried at
202 40 °C, weighed, washed and sieved with mesh widths of 63 µm and 150 µm. Isotope
203 measurements were made on the planktonic foraminifera *Globigerinoides ruber* var.
204 *alba* (20 specimens per sample), which were hand-picked from the > 150 µm size
205 fraction.

206 The isotopic composition of carbonate was measured according to the method
207 described in detail in Breitenbach and Bernasconi (2011). Briefly, approximately 60-
208 80 µg of crushed, homogenized foraminifera shells were added to 4.5 ml Exetainers,
209 (Labco, High Wycombe, UK) and flushed with pure helium. The samples were
210 reacted with 3-4 drops of 100% phosphoric acid at 70 °C with a Thermo Fisher
211 GasBench device connected to a Thermo Fisher Delta V mass spectrometer. The
212 average long-term reproducibility of the measurements based on replicated
213 standards was ±0.06‰ for $\delta^{18}O$. The instrument was calibrated with the international
214 standards NBS19 ($\delta^{18}O$ = -2.2‰) and NBS18 ($\delta^{18}O$ = -23.01‰). The isotope values
215 are reported in the conventional delta notation with respect to VPDB (Vienna Pee
216 Dee Belemnite).

217 The age model of MD04 2723 was established by correlation of the oxygen isotope
218 record with the Eastern Mediterranean *G. ruber* stack of Wang et al. (2010) using the
219 Software Analyseries (Paillard et al. 1996).

220 2-2-3 Total organic carbon

The sediment samples were freeze-dried, crushed and homogenized for geochemical analysis (total organic carbon, Ca and Br contents). For the analysis of total organic carbon, sediment samples were acidified by H_3PO_4 (1 M) to remove carbonates, dried on a hot plate at 40 °C, and measured by combustion in a LECO CS 300 carbon sulfur analyzer. Two or three replicates of dried and homogenized sediment (50 mg) were analyzed per sample.

2-2-4 Rock-Eval pyrolysis

All samples were analyzed with the Rock-Eval thermal analysis technique, using a RE6 Turbo device (Vinci Technologies). Details of the RE6 apparatus are extensively described in Behar et al. [2001]. Analyses were carried out using the operating principles for the analysis of recent marine sediments. [Baudin et al., 2015]. The RE6 technique provided measurements from the sequential pyrolysis and oxidation of approximately 40 mg of desalted crushed sample. The pyrolysis gas effluents (mainly hydrocarbons) were detected and quantified by flame ionization detection (FID), and the evolution of CO and CO_2 gas was quantified by infrared detection during the pyrolysis and oxidation stages. The pyrolysis was carried out from 180 °C to 650 °C in an N_2 atmosphere, whereas the oxidation was carried out from 300 °C to 850 °C in a laboratory air atmosphere.

The RE6 technique provides information on the quantity, type (sources) and thermal evolution state of sedimentary organic matter.

2-2-5 Bromine and calcium analysis on single samples

The bromine and calcium contents were analyzed by X-ray fluorescence using an xSORT instrument (Spectro Ametek). The instrument was set up on a stand, and analyses were performed with the manufacturer's Environ-H program. Ground

sediment was placed in a 15 mm diameter plastic cup with a 4 µm thick polypropylene window and was manually compacted. For each sample, four replicates were analyzed during 300 s.

For Ca, 25 eastern Mediterranean sediment samples analyzed by ICP-AES (Service d'Analyses des Roches et Minéraux, SARM - Nancy). A range of concentrations from 3 to 10% was used to calibrate the equipment. The detection limit was 50 ppm, and the replicates agree within 5%.

For Br, we used standards prepared from a Mediterranean sediment for calibration. The sediment was sieved with a mesh width of 40 µm and high purity water, freeze-dried, crushed and homogenized. Known quantities of KBr solution were added to the sediment subsamples, and the subsamples were freeze-dried, crushed and homogenized. The detection limit was 5 ppm, and the replicates agreed within 5%.

The samples were also analyzed for calcium and total bromine (BrTot). Part of the samples was then rinsed twice with ultrapure water to remove residual salt from marine pore-water evaporation. A second analysis was carried out to analyze solid-phase bromine (BrSol). Previous studies have shown that pure water removes Br only to the extent that would be expected from dried interstitial water [Harvey, 1980; Mayer et al., 1981; Mayer et al., 2007] and that insignificant organic bromine was washed away [Mayer et al., 2007].

2-2-6 Bromine and calcium analysis by core scanner

High-resolution geochemical elemental composition records were measured directly on the archive slab surface with an Avaatech XRF Core Scanner at the EPOC Laboratory (University of Bordeaux). After cleaning and preparation of the slab surface, three separate runs (10, 30 and 50 kV, with currents of 0.6, 1.5 and 2.0 mA,

respectively) were performed every 5 mm down-core with a down-core slit size of 5 mm. Sampling time was set to 10 s at 10 kV, 15 s at 30 kV and 20 s at 50 kV. The slab surface was covered with a 4 µm thin SPEXCerti Prep Ultralene1 foil to avoid contamination of the XRF measurement unit and desiccation of the sediment. Raw data spectra were processed by the analysis of the X-ray spectra using the iterative least squares software (WIN AXIL) package from Canberra Eurisys. The elements analyzed include a broad range, from aluminum ^{13}Al through uranium ^{92}U (Richter et al, 2006, Tjallingii, 2007). In this paper, we focused on select elements, such as calcium (Ca) and total bromine (BrTot).

To transform core scanner relative data into quantitative results, 56 sediment samples were selected within areas of the core scanner signal stability (at least 2 cm). Despite uncertainty linked to the variability of the water content, significant correlations were highlighted between the core scanner data on wet sediment samples and the X-ray fluorescence results on dried sediment samples (BrTot, r = 0.95; Ca, r = 0.93).

2-2-7 Characterization of clay minerals

Sediments were gently crushed, and part of the collected powder (grain size less than 50 µm) was added to deionized water to form mineral suspensions, which were dispersed ultrasonically for 2 minutes. The less than 2 µm fraction size of the sediments was collected by sedimentation, and clay minerals were characterized from the XRD patterns of the oriented preparations acquired in air-dried conditions and after ethylene glycol solvation. XRD analyses were performed using a Bruker® D8 XRD diffractometer (CuKα radiation). Diffracted beam Cu$K\alpha^{1+2}$ radiation was used (40 kV, 40 mA) and collected by a linxeye detector. Relative humidity was not controlled during data acquisition. The oriented preparation of the less than 2 µm

fraction size was analyzed from 2º to 30º 2θ for a detailed characterization of the d00□ reflections of phyllosilicates.

Petrographic studies were performed on the rock fragments using a JEOL 5600 LV SEM equipped with an EDS (BRUKER XFlash 4030 Silicon drift detector). SEM observations were performed in secondary electron imaging mode (SEI) for morphological investigations and backscattering electron mode (BSE) on carbon-coated thin sections for imaging of the chemical contrast and selection of local sites for punctual chemical analysis. The analytical conditions were 15 kV, 1 nA, a counting time of 60 s and a working distance of 16.5 mm. The standards used for EDS consisted of albite (Na, Al, Si), almandine (Mg, Fe), diopside (Ca), orthoclase (K) and spessartite (Mn). Matrix corrections were performed using an integrated program (a PhiRhoz correction). The reproducibility of the standard analyses was nearly 1.5% for all of the elements, except Na, which had a reproducibility of 3%.

TEM-EDX microanalyses were conducted on individual particles deposited on a C-coated copper grid using a JEOL JEM 2011 TEM fitted with an X-Flash Silicon Drift Detector 5030 (Bruker). The data collection parameters were set as follows: magnification of 50000 x, 4 L spot size, angular tilt of 20° toward the detector, time constant of 60 kcp.s^{-1}, energy range of 40 keV, and corrected counting time of 30 s. The beam diameter was set to ~20 nm to reach the smallest particles.

The mid-infrared (MIR) spectra (400 to 4000 cm^{-1}) were acquired on KBr pellets using a Nicolet 760 FTIR spectrometer equipped with a potassium bromide (KBr) beamsplitter and a DTGS-KBr detector. The resolution was set to 4 cm^{-1}, with a co-addition of 100 scans. KBr pellets contained 1 mg of sample for every 150 mg of KBr powder, which was crushed into a mortar and pressed under 8 tons for 5 minutes in a hydraulic press before drying at 120 °C.

2-2-8 Quantification of the relative amounts of kaolinite and smectite

The relative amounts of kaolinite and smectite (smectite/kaolinite ratio) of the natural samples were obtained from normalized near infrared spectra according to the methodology described by Hébert et al. [2015]. Near-infrared spectra were collected in reflectance mode using a Nicolet 750 FTIR spectrometer with an integration sphere accessory. The spectrometer was equipped with a white light source, a CaF_2 beam splitter and a PbSe detector. Spectra over the 10000-4000 cm^{-1} wavenumber range were obtained by co-addition of 100 spectra with 4 cm^{-1} resolution. For measurements, a few hundreds of milligrams of samples were either placed directly onto the integration sphere's shutter or disposed into IR-transparent flasks when unconsolidated.

Kaolinite and smectite have several atomic bonds within their crystal structure that absorb radiation in the near-infrared domain. The absorption bands of kaolinite and smectite can be observed in two regions of the infrared spectrum: from 1350 to 1500 nm (for overtones of OH stretching vibrations) and from 2100 to 2400 nm (for the combination of OH stretching and bending vibrations). The absorption bands of kaolinite and smectite overlap in the two regions of interest. However, kaolinite has a diagnostic absorption feature at 2165 nm, and the relative proportions of smectite and kaolinite can be determined by deconvolution of the four infrared (IR) bands that are overlapped in the region between 2100 nm and 2300 nm (Hébert et al., 2015). The smectite/smectite+kaolinite ratio calculated using this method corresponds to the percentage of smectite in the clay material, which will be referred to as Sm% hereafter.

342 2-2-9 Statistical analysis

343 Because each variable in the datasets used here can contain error [Laws and Archie,
344 1981; Sokal and Rohlf, 2012], we applied Model II regression to determine the
345 correlations between the studied variables. This model prevents underestimation of
346 the regression slope [Riker, 1973]. Regression analysis was performed using the
347 lmodel2 package from R language (R Development Core Team, 2013). The statistical
348 level of significance was defined at $p<0.05$ (Spearman's rank correlation test).

349 3 Results

350 3-1 Sediment characteristics

351 The stratigraphic framework was established based on the $\delta^{18}O$ isotopic record (Fig.
352 2). The core displays a complete record of the last 1080 ky. According to the very low
353 maximal burial depth reached by these sediments (the core length is only 36.5 m),
354 physical parameters, such as temperature and pressure, did not significantly
355 influence the evolution of the studied parameters during the burial history.

356 Deposits are characterized by cyclic sedimentation of organic-rich sapropel layers
357 and organic-poor hemipelagic to pelagic sediments. Based on the sediment
358 thickness, and without considering the upper sediment column (0-6.5 m), which was
359 stretched by coring, the sedimentation rate varies slightly between 3.5 cm ky^{-1} (6.5-
360 20.0 m) and 2.8 cm ky^{-1} (20.0-36.5 m). The Ca concentration varies from 3.2 to
361 22.4%, which corresponds to a carbonate content of 8 to 56% (Fig. 2). The upper
362 part of the core (0-493 ka) displays slightly higher values, with a mean of 11.9%, than
363 the lower part (493-1084 ka), with a mean of 10.5%. Thus, the Ca content exhibits a
364 weak but significant anticorrelation with age (N=7250, r=-0.23).

365 According to the discrete occurrence of sapropels in the sedimentary column, the
366 organic carbon content has high variability (0.17 to 6.74%, S5 sequence for example)
367 on a small scale (10 to 20 ky) but is stable on a 1 my scale (Fig. 2). Correlation tests
368 prove that the TOC and age are independent variables (N=323, r=-0.08). The
369 quantity of organic matter is constant through time.

370 Rock-Eval pyrolysis was originally developed to characterize the organic matter
371 present in oil source rocks [Espitalié et al., 1977], which are typically more thermally
372 mature and at higher concentrations than thermally immature marine sediments, like
373 the Mediterranean sapropels. Rock-Eval analyses have proved valuable in helping to
374 determine organic matter sources and the state of diagenetic transformation in
375 immature sediment samples [Bouloubassi et al., 1999; Baudin et al., 2007;
376 Tribovillard et al., 2008; Hatcher et al., 2014]. The hydrogen (HI) and oxygen indexes
377 (OI) are related to the atomic composition of the total organic matter and are
378 commonly plotted against each other in a modified van Krevelen-type plot (Fig. 3), in
379 which three main types of organic matter and their thermal alteration routes are
380 defined [Tissot and Welte, 1984].

381 The oxidation of organic matter affects both the HI and OI. As marine organic matter
382 (Type II) is oxidized, there is a shift to lower HI and higher OI, and the HI-OI plot
383 approaches the characteristics of Type III vascular plant organic matter [Bouloubassi
384 et al., 1999 on the eastern Mediterranean ODP site 969]. The results of the Rock-
385 Eval analyses of sapropels from MD04 2723 exhibit a similar trend (Fig. 3). High
386 organic carbon sapropel samples correspond to marine Type II organic matter that is
387 well preserved and lower organic carbon to mainly altered marine organic matter.
388 Microbial alteration of the organic matter during sinking or in the upper sediment
389 layers, particularly by sulfate-reducing bacteria, has been reported to reduce the HI

390 [Vetö et al., 1994]. The significant positive correlation between HI and TOC supports
391 this interpretation (N=20, r=0.89).

392 3-2 Bromine

393 BrTot varies from 32 to 344 ppm, with a mean of 74 ppm (Fig. 2). This variability
394 reflects the variation in the organic matter content; higher BrTot concentrations
395 correspond to sapropel layers. Statistical analysis of the dry sediment samples shows
396 a significant correlation (N=323, r=0.90) between BrTot and TOC. Despite this BrTot-
397 TOC correlation, a slight but significant evolution can be shown with the age
398 (N=7250, r=-0.22). Without the sapropel layers, the anticorrelation is weaker
399 (N=6335, r=-0.17). BrTot decreases through time, while TOC is constant.

400 To further explore this debromination, particular attention is paid to solid-phase
401 bromine (BrSol). BrSol and TOC display a highly significant relationship (N=63,
402 r=0.92) (Fig. 4 and Tab. 1).

403 The intercept of the all data regression lines tend towards zero. This proves that
404 BrSol is bromine linked to organic matter (BrOrg). This direct correlation between the
405 bromine content and the organic carbon content of marine sediments has been
406 demonstrated by several authors [Price et al., 1970; Price and Calvert, 1977;
407 Pedersen and Price, 1980; Martin et al., 1993; Ziegler et al., 2008; Leri et al., 2010].

408 The BrOrg results are in close proximity for low TOC contents and become more
409 scattered with increasing TOC. This dispersion can be explained by the age of the
410 samples. The more recent sapropelic sequences exhibit higher BrOrg than the older
411 ones at equivalent TOC concentrations. The analysis of this issue by sapropelic
412 sequences is presented in Table 1.

413 The correlations are highly significant for the S1, S5, S17 and S28 sequences. The
414 numbers of samples are too low for the S9, S10 and S12 sequences; therefore, the
415 correlations are not statistically valid. Nevertheless, the different sequences display a
416 consistent trend of a decreasing slope with age (Fig. 5).

417 However, it remains to be determined whether the organic carbon content can affect
418 debromination. To highlight this possibility, we selected 4 data sets corresponding to
419 different TOC ranges and examined the evolution of BrOrg through time for each of
420 them (Fig. 6 and Tab. 2). We chose narrow ranges of TOC (0.5 to 0.8%) and, when
421 possible, a broad range of ages.

422 Organic-poor samples (TOC<0.5%) do not show significant evolution through time
423 (N=16, r=-0.17, NS), i.e., our dataset does not allow us to demonstrate a change with
424 age. BrOrg is always low and remains almost constant.

425 In contrast, the 1.5-2.3% and 2.3-3% TOC ranges show significant linear correlations
426 of BrOrg with age, i.e., the higher the TOC range, the steeper slope, and the higher
427 correlation coefficient (Table 2).

428 The rate of debromination (DBrR) increases with TOC content. For a mean TOC of
429 0.24%, BrOrg is almost stable (it varies from <5 to 12 ppm during 1 my). DBrR
430 cannot be calculated, but is low. For a mean TOC of 1.83%, BrOrg decreases from
431 68 to 40 ppm in 1 my, and DBrR = 2.3×10^{-4} µmolBrOrg molC^{-1} y^{-1}. For a mean TOC
432 of 2.73%, BrOrg decreases from 147 to 32 ppm in 1 my, and DBrR increases to $6.3 \times$
433 10^{-4} µmolBrOrg molC^{-1} y^{-1}.

434 For an organic carbon content greater than 4%, the data are scarce. Only five
435 sapropel layers reach this level of TOC, and long periods of time are without data
436 (Fig. 2). Compared to the other ranges studied, the variability of BrOrg is greater for

437 samples of similar TOC and age and outliers appear. The results obtained for the full
438 range (4.0-6.5%) are comparable to those derived from the more limited ranges
439 (4.55-4.95% and 5.4-6.4%). However, the slopes of the calculated regression lines
440 are lower than that for the 2.3-3% TOC range, approximately -0.07. There is an
441 unexpected decrease in the rate of debromination to approximately 2.0 x 10^{-4}
442 µmolBrOrg $molC^{-1}$ y^{-1}.

443 The intercepts provide an indication of the initial quantity of BrOrg, i.e., the quantity at
444 the time of deposit, so it is possible to calculate the initial value of BrOrg/TOC (Table
445 2). For the <0.5% range, the initial BrOrg/TOC (weight ratio 29 x 10^{-4}, molar ratio 4.4
446 x 10^{-4}) is in accordance with the value of the younger sample (weight ratio 30 x 10^{-4},
447 molar ratio 4.5 x 10^{-4}, for 2 ka). Likewise, for the 1.5-2.3% range, the initial
448 BrOrg/TOC (weight ratio 37 x 10^{-4}, molar ratio 5.6 x 10^{-4}) is in accordance with the
449 value of the younger sapropel (N=4, weight ratio 37.8 x 10^{-4}, molar ratio 5.7 x 10^{-4} for
450 8 ka). For the higher TOC ranges, the youngest samples are too old for a valuable
451 comparison. For the 2.3-3.0% range, the initial calculated BrOrg/TOC is increasing
452 (weight ratio 54 x 10^{-4}, molar ratio 8.1 x 10^{-4}). However, for higher TOC (4.0-6.5%
453 range) the initial calculated BrOrg/TOC is decreasing (weight ratio 37 x 10^{-4}, molar
454 ratio 5.6 x 10^{-4}).

455 The solid-phase organic bromine-age relationship holds in the organic-rich
456 sediments, whereas it fails in the organic-poor sediments

457 3-3 Clay minerals

458 The bulk clay mineralogy of the organic-rich and organic-poor sediments is similar all
459 along the investigated core material. The XRD patterns obtained from the oriented
460 mounts of the less than 2 µm fraction size of the sediments indicate that their clay

461 material is primarily a mixture of smectite and kaolinite, with minor amounts of micas
462 [muscovite] and subordinated chlorite. Similar clay mineralogical composition has
463 been described on the Nile margin [Maldonado and Stanley, 1981; Stanley et al.,
464 1998; Hamann et al., 2009]. Smectite predominates in all samples. It was identified
465 from its broad d_{001} reflection toward 15 Å in the air-dried preparation of Ca-saturated
466 samples that expands to 17 Å and the occurrence of a harmonic d_{002} reflection close
467 to 8.5 Å after saturation with ethylene glycol (Fig. 7).
468 The large width at half maximum height (FWMH > 1.5°2θ) of the d_{001} reflection and
469 the very low intensity of the d_{002} reflection of the smectite after ethylene glycol
470 saturation (which makes it difficult to identify in the XRD pattern) is indicative of the
471 low coherent scattering domain size (CSDS) of smectite crystallites. Kaolinite is
472 characterized by typical d_{001} and d_{002} reflections at 7.16 Å and 3.57 Å, respectively.
473 From a comparative study of the XRD patterns of all samples, it can be observed that
474 the intensity ratio between the d_{001} reflections of smectite and kaolinite significantly
475 varies all along the sapropelic sequence.
476 SEM observations indicate that very fine-grained clay particles (less than 2 µm) are
477 intimately mixed with calcareous micro- to nano-fossil oozes, particles of
478 carbonaceous material and very fine-grained detrital mineral, such as micas, alkali
479 feldspars and quartz. The authigenic minerals identified by petrographic observation
480 consist only of spherical aggregates of octahedral pyrite (framboidal pyrite), which is
481 very common within the organic-rich sediments (Fig. 8), and tiny crystals of
482 manganese oxides that have been observed locally in proximity to the sapropelic
483 horizons.
484 When observed after dispersion in water and sedimentation on a glass substratum
485 (Fig. 8b), the clay particles present a typical morphology of smectite (i.e., resulting in

the aggregation of thin films of clay minerals with anhedral morphology) intimately associated with more dispersed subhexagonal plates of kaolinite. HRTEM observation of the smectite tactoids indicates that they are composed of very thin crystallites, which display a very small number of stacked individual layers (less than 5) when oriented perpendicularly to c* (Fig. 8c). This is in agreement with the XRD data, which indicated the low coherent scattering domain size (CSDS) of the smectite crystallites.

The crystal-chemical characteristics of the smectite particles do not change significantly along the investigated core. Despite a relatively large range of chemical variation, which results from intimate mixing with different types of mineral impurities, the punctual analyses obtained from SEM-EDX and TEM-EDX converge toward a composition of montmorillonite (Table 3).

All structural formulas are characteristic of dioctahedral smectite with octahedral occupancy ranging from 2 to 2.1 atoms per formula unit (a.p.f.u.), in which the tetrahedral negative charge (due to substitution of Al with Si) is very low (less than 0.2). Despite the uncertainty in the partitioning of Mg between the octahedral sheet and interlayer position and the Fe^{2+}/Fe^{3+} ratio within the octahedral sheet, the negative charge of the 2:1 layer is due to Mg^{2+} for Al substitution. The montmorillonitic composition of the smectite of both organic-rich and organic-poor sediments is confirmed by the middle-infrared spectra of the clay material. The OH bending bands of the phyllosilicates between 820 and 915 cm^{-1} agree with the dioctahedral nature of the clay minerals (kaolinite and smectite) contained in the sample [Farmer, 1974]. Both kaolinite and smectite contributed to the 912 cm^{-1} band, which was attributed to an AlAl-OH vibration. The 875 and 835 cm^{-1} absorption bands

510 were attributed to $AlFe^{3+}$-OH and $AlMg^{2+}$-OH bending vibrations, respectively
511 [Farmer, 1974, Petit and Decarreau, 1990, Petit et al., 2002].
512 The quantitative analysis of the relative amounts of smectite and kaolinite in the bulk
513 samples by NIR spectrometry (Figure 9) confirms that smectite largely predominates
514 over kaolinite all along the investigated core.

515 The range of variation of the percentage of smectite in the clay material (Sm%) is
516 restricted between 62 and 97% (Fig. 2), and no clear variation can be observed in a
517 comparison of the S/K ratios in the different compartments of the studied core. The
518 range of variation of the Sm% determined at the scale of the sapropelic sequence is
519 often not far from that measured at the core-scale. The smectite content variability
520 cannot be linked to organic matter content variation, and TOC and Sm% are two
521 relatively independent parameters (N=191, r=-0.22, highly significant). The most
522 significant variation of Sm% observed at the core scale is an increase in the smectite-
523 rich samples (Sm%>90) from the bottom (oldest sediments) to the top (younger
524 sediments) of the investigated core.

525 4 Discussion

526 4-1 Debromination

527 There are many ways to explore debromination.

528 One way is BrTot high-frequency core scanner analysis (Fig. 2). Total bromine
529 consists of dissolved bromine and solid-phase bromine. The solid-phase bromine is
530 linked to organic matter and immobilized, but it progressively leaves the organic
531 matter and is released as bromide into pore water. Therefore, it decreases with age.
532 The dissolved bromine is composed of two components: (1) bromide provided by
533 marine pore-water salt at the time of deposition and debromination and (2) organic

534 bromine. No significant chemical uptake processes are known to act as a sink for
535 bromide [Berg and Solomon, 2016]. Without the influence of other processes, BrTot
536 will remain constant. However, dissolved bromine is mobile. When debromination
537 occurs, the bromide concentration increases in the pore water more strongly in the
538 organic-rich layers than in the organic-poor layers. As a result, bromide is firstly
539 transported by diffusion from organic-rich to organic-poor sediment to equalize the
540 concentrations. On a larger timescale, bromide migrates through diffusion and/or
541 advection back toward the overlying ocean. The end result is that BrTot and its
542 variability range decrease with age, even though the bromide/chloride ratio increases
543 with depth [Berg and Solomon, 2016]. The MD04 2723 core scanner data exhibits
544 this general trend, whereas TOC remains constant at the same timescale, which
545 supports the debromination of the organic matter and the upward bromide migration.

546 However, BrTot and bromide/chloride ratio analysis provide a limited estimation of
547 debromination itself. Another way to obtain more accurate values is to compare BrTot
548 and the organic carbon content of organic-rich sediment layers. When TOC is high,
549 BrTot is mainly composed of bromine linked to organic matter and the pore-water
550 bromide can be neglected. The core MD04 2723 contains two highly organic-rich
551 sapropel layers: S5 and S28 (Fig. 2). They have similar maximum TOC contents
552 (6.7% for S5 and 6.4% for S28) and different BrTot maximum concentrations (326
553 ppm for S5 and 174 ppm for S28). The debromination rate can be estimated at 3.5 x
554 10^{-4} µmolBrOrg $molC^{-1}$ y^{-1}, in accordance with results obtained directly by the BrOrg
555 measurements (Tab. 2).

556 Studying BrOrg variability is a better way to obtain accurate values of the
557 debromination rates. There are two pathways acting simultaneously in biological
558 systems for the production of BrOrg, biotic production in cells of macro and

559 microalgae as a result of the enzymatically mediated reaction of Br^- and abiotic
560 production by nucleophilic substitution [Ballschmiter, 2003]. These reactions produce
561 aliphatic and aromatic forms of organobromine [Leri et al., 2014]. During organic
562 matter degradation, bromine can be removed from organobromine compounds
563 through microbial metabolic or abiotic debromination processes. One metabolic
564 pathway in the degradation of organic material is organohalide respiration. Bacteria
565 in anoxic environments utilize reductive dehalogenase to break the carbon-halogen
566 bond of organohalide compounds functioning as electron acceptors. The bromine is
567 replaced by a hydrogen atom. It has been hypothesized that this metabolic pathway
568 using reductive dehalogenase may be an important energy source for microbial
569 communities in the deep biosphere [Futagami et al., 2009]. The energy yield of
570 organohalide respiration in the natural environment can be several times greater, on
571 a per mole basis, than other metabolic pathways, such as sulfate reduction and
572 methanogenesis [Dolfing, 2003]. Bacterial groups that have the potential to use
573 organohalide respiration as a metabolic pathway have been found to be abundant in
574 deep subsurface marine sediments, both geographically and with depth [Futagami et
575 al., 2009; Orcutt et al., 2011]. Less is known about organohalide fermentation, but it
576 has been shown to be another potential energy-producing pathway for microbes in
577 the deep biosphere [Justicia-Leon et al., 2012; Lee et al., 2012]. Based on the BrOrg
578 concentration variability, we have demonstrated that the rates of debromination are
579 linked to the TOC contents. They increase from less than 2.3×10^{-4} µmolBrOrg $molC^{-1}$ y^{-1}
580 up to 6.3×10^{-4} µmolBrOrg $molC^{-1}$ y^{-1} when TOC varies from 0.17 to 3%. For
581 higher TOC values, precise rates of debromination could not be reliably established
582 due to scattered data (Fig. 6), but they decrease in all cases. To explore the
583 relationship between TOC and the rate of debromination, two assumptions are

584 proposed: the rate of debromination depends on microbial activity and/or the
585 bioavailability of organic matter. Cragg et al. (1998) studied the bacterial
586 concentrations at the eastern Mediterranean ODP site 969, which has similar cyclic
587 sedimentation of organic-poor and organic-rich (80 sapropels beds to 116 mbsf)
588 sediments. Within the range of TOC concentrations usually encountered in marine
589 sediments (0-3%), the data set produced a significant correlation between TOC and
590 bacterial populations, in good agreement with the general profile derived from other
591 ODP sites. The addition of data with higher TOC destroyed the relationship, which
592 suggests that at high concentrations, such as those found in sapropels, TOC is
593 effectively present in excess and ceases to be a limiting factor for bacterial population
594 size. The remarkable fact that the bacterial populations and rates of debromination
595 both increase with the TOC concentration but only within the 0-3% range suggests
596 that debromination is quantitatively dependent on microbial activity. However, it is
597 difficult to explain why the TOC concentration does not behave as a limiting factor
598 when its content is greater than 3%. Cragg et al. (1998) suggested that organic
599 carbon within the sapropel layers must be predominantly recalcitrant and only slowly
600 bioavailable.

601 The organic carbon content of the sapropel layers depends on the rate of
602 degradation/preservation of organic matter. During sapropelic periods, the water
603 column is stratified. The upper layer is normally oxygenated, and aerobic organic
604 matter degradation by microorganisms occurs. The lower layer is oxygen-depleted,
605 and organic matter is oxidized through various less-effective anaerobic pathways
606 [Demaison and Moore, 1980; Emerson and Hedges, 1988]. We assume that very
607 stable stratification results in a high-TOC sapropel (more than 3%), and low organic
608 carbon sapropels correspond to instable stratification with periodic reoxygenation of

609 the entire water column [Casford et al., 2003; Stefanelli et al., 2005 and Meyers et al.,
610 2006; Rohling et al., 2015]. The two degradation pathways produce different organic
611 molecules, which are less bioavailable in the case of oxygen-depleted conditions.
612 Therefore, in organic carbon-rich sapropels (TOC > 3%) organic matter would not be
613 as bioavailable as in low organic carbon sapropels (TOC < 3%). Furthermore, the
614 initial BrOrg/TOC also decreases at the 3% TOC. The sediments with 2.3-3.0% TOC
615 provide ideal conditions for the development of bacterial groups that may have the
616 potential to use organohalide respiration: a high content in Br-rich organic matter.
617 Sediment with higher TOC has higher BrOrg content but a lower initial BrOrg/TOC
618 and could be less attractive.

619 However, some factors of the debromination rate variability for very high organic
620 carbon content remain to be identified. We need to explain why two samples
621 collected 3 cm apart within the same sapropel (S17) with the same TOC
622 concentration (4.7 and 4.8%) present different BrOrg contents (140 and 86 ppm). The
623 first cited sample follows the general debromination trend, whereas the second
624 displays evidence of a higher rate (Fig. 6). Therefore, sometimes high rates of
625 debromination occur, even for high organic carbon content layers. The explanation of
626 this difference does not lie in the burial conditions, which are the same. Rather, the
627 solution is in the initial organic matter quality, which is dependent on the production
628 and/or degradation conditions. A 1 cm thick sample corresponds to three centuries of
629 basin history, a duration cannot analyze the climatic variability of the temperature
630 sea-surface, Nile floods or depth of the oxic/anoxic water interface, three parameters
631 that may have influenced the quality of the produced and preserved organic matter
632 [Meyers, 2006]. Sapropels are organic-rich layers, but for most of them, preserved
633 organic matter represents a small portion of the produced organic matter. For low

TOC content sapropels (1-3%), the initially produced marine organic matter is mainly degraded. Thus, the degradation step plays a major role in the quality of the finally preserved organic matter. In contrast, for higher organic carbon sapropels, even if the degradation pathways remain important, a higher proportion of produced organic matter is preserved and the quality of the produced organic matter is a more important factor in the variability of bioavailability.

4-2 Clay mineral evolution

The core MD04 2723 provides an opportunity to examine the evolution of layer silicates in parallel to that of organic matter during the last million years of sedimentation and eogenesis of sediments in the eastern part of the Egyptian continental margin. Kaolinite and smectite are known to be the diagnostic clay minerals of the eogenesis of mudstones (Burley, 1993 and references therein). However, it is unclear whether these clay minerals originate from sedimentation (detrital clays) and/or from the eogenesis of the sediments during their incipient burial.

This study shows that (1) there is no evidence of authigenic clay minerals and that (2) dioctahedral smectite largely predominates over kaolinite in the samples collected all along the core MD04 2723. More specifically, infrared spectroscopy and microchemical analyses indicated that the crystal chemistry of the dioctahedral smectite agrees with that of montmorillonite. Its mineralogical and chemical composition is similar to that of the smectite previously identified in the Nile suspended matter [Dekov et al., 1997] and the Nile alluvial soils in Egypt [Kishk et al., 1976] and the range of Sm% measured all along the core is in full agreement with the published clay mineral data from the Nile assemblage [Hamann et al., 2009]. On the basis of the qualitative analysis in this study, it is assumed that the clay mineralogy of

659 the core MD04 2723 is essentially representative of the detrital Nile source. However,
660 on the basis of quantitative analysis, Sm% variability is likely to occur at two different
661 timescales.

662 Some sapropelic sequences exhibit a wide range of variation in Sm% (S10, for
663 example, 71-97%, Fig. 2) while others do not (S15, for example, 66-73%, Fig. 2). The
664 highest Sm% can be located either in the organic-rich (S10 and S11 sequences) or in
665 the organic-poor (S7 and S9 sequences) sequences. The controlling factor of the
666 Sm% variation is not climatic because all four aforementioned sapropels correspond
667 to low values of the $\delta^{18}O$ isotopic record. As expected from the absence of diagenetic
668 evolution of clay minerals, the smectite concentration and TOC are not correlated.

669 Over a span of one million years, a slight change occurs, which is highlighted by the
670 mean values for each sapropelic sequence (Fig. 10).

671 The lower part of the core (500 to 1080 ka) is characterized by a nearly constant and
672 low (69-73%) Sm%, whereas the upper part is characterized by heterogeneous mean
673 values with successively increasing or decreasing gradients (Sm% between 71 and
674 88%), which cannot be linked to the $\delta^{18}O$ isotopic record. The 500 ka limit also
675 affects others sedimentary parameters, such as the Ca concentration and
676 sedimentation rate. The last 500 ky shows an increase in the sedimentation rate, the
677 carbonate content and the Sm% variability. Even though the cause of these
678 variations remains uncertain, the hypothesis of temporal change in detrital sources
679 can be invoked.

680 5 Conclusion

681 The studied site displays both a high degree of stability in the organic supply at a
682 one-million-year scale and great variability in the organic matter preservation at a 10

683 ky scale, an ideal situation to highlight and discuss the influence of the organic matter
684 content on the mineralogical and geochemical evolution during eogenesis. This
685 allows us to demonstrate that at a one-million-year scale, the organic matter content
686 has no significant influence on clay eogenesis. Detrital smectite and kaolinite remain
687 unchanged everywhere, even within the sapropels where high bacterial populations
688 are active.

689 We have demonstrated that solid-phase BrOrg is a reliable tracer of debromination
690 rates in marine sediments. Based on the highly variable TOC concentration of the
691 eastern Mediterranean sea, it was determined that the rates of debromination
692 depend on the organic matter content. This observation provides the basis for further
693 investigation of other oceanic basins. Within the range of TOC concentrations usually
694 encountered in marine sediments (0-3%), both bacterial populations and the rates of
695 debromination increase with TOC content. It can be assumed that these two
696 parameters are correlated. The increase in bioavailable organic matter induces
697 growth of active bacterial populations, resulting in higher rates of debromination. In
698 the eastern Mediterranean sea, the depth profile of the bacterial populations is in
699 good agreement with the general profile derived from other oceans [Cragg et al.,
700 1998; Parkes et al., 2014]. This suggests that the rates of debromination obtained in
701 the Mediterranean sea are relevant for all ocean basins. This assumption should be
702 supported by further investigations, which could be performed on a basin that
703 displays a high and stable organic carbon content over time. This approach would
704 provide only one rate of debromination. It would be more interesting to search for a
705 Mediterranean-like basin that exhibits both a high degree of stability of the organic
706 supply at a one-million-year scale and great variability in the organic matter content
707 at a 10 ky scale. Different rates of debromination could be investigated. Extending

the time-range of the sedimentation and diagenetic evolution to a ten-million-year scale would show whether clay minerals remain stable over a one-million-year scale due to of slow reaction kinetics.

Acknowledgements

This work was funded by the French program “Action Marges”. We thank Jean Mascle and the on-board scientific team for their assistance and Yvon Balut and the Marion Dufresne II crew (French Polar Institute: IPEV) for technical support during the Vanil cruise.

References:

ARNDT S., JØRGENSEN B.B., LAROWE D.E., MIDDELBURG J.J., PANCOST R.D. & REGNIER P. (2013). - Quantifying the degradation of organic matter in marine sediments: A review and synthesis. - *Earth-Science Reviews*, **123**, 53–86

BALLSCHMITER K. (2003). - Pattern and sources of naturally produced organohalogens in the environment: biogenic formation of organohalogens. - *Chemosphere*, **52**, 313–324.

BARNES M. A., BARNES W.C. & BUSTIN R. M. (1990). - Chemistry and diagenesis of organic matter in sediments and fossil fuels. *In:* Geoscience Canada Reprint Series, Diagenesis, 189-204.

BAUDIN F., COMBOURIEU-NEBOUT N. & ZAHN R. (2007). - Signatures of rapid climatic changes in organic matter records in the western Mediterranean Sea during the last glacial period. – *Bull. Soc. Géol. Fr.*, **178**, 1, 3-13.

731 BAUDIN F., DISNAR J.P., ABOUSSOU A. & SAVIGNAC F. (2015). - Guidelines for
732 Rock–Eval analysis of recent marine sediments. – *Org. Geochem.*, **86**, 71–80.

733 BEHAR F., BEAUMONT V. & DE PENTEADO, H.L. (2001). - Rock–Eval 6
734 technology: performances and developments. - *Oil and Gas Science and*
735 *Technology,* **56**, 111–134.

736 BERG R.D. & SOLOMON E.A. (2016). - Geochemical constraints on the distribution
737 and rates of debromination in the deep subseafloor biosphere. – *Geochim.*
738 *Cosmochim. Acta*, **174**, 30–41.

739 BÉTHOUX J.P. & PIERRE C., (1999). - Mediterranean functioning and sapropel
740 formation: respective influences of climate and hydrological changes in the Atlantic
741 and the Mediterranean. - *Mar. Geol.,* **153**, 29–39.

742 BOULOUBASSI I., RULLKÖTTER J. & MEYERS, P.A. (1999). - Origin and
743 transformation of organic matter in Pliocene–Pleistocene Mediterranean sapropels:
744 organic geochemical evidence reviewed. - *Mar. Geol.,* **153**, 177–197.

745 BREITENBACH S.F.M. & BERNASCONI S.M. (2011). - Carbon and oxygen isotope
746 analysis of small carbonate samples (20 to 100 µg) with a GasBench II preparation
747 device. - *Rapid Communications in Mass Spectrometry,* **25**, 1910-1914.

748 BURLEY S. D. (1993). - Models of burial diagenesis for deep exploration plays in
749 jurassic fault traps of the central and Northern North Sea. - *Geological Society,*
750 *London, Petroleum Geology Conference series 1993*, **4**, 1353-1375.

751 CASFORD J.S.L., ROHLING E.J., ABU-ZIED R.H., JORISSEN F.J., LENG M. &
752 THOMSON J. (2003). A dynamic concept for eastern Mediterranean circulation and

753 oxygenation during sapropel formation. - *Palaeogeogr. Palaeoclimatol. Palaeoecol.*,
754 **190**, 103–119.

755 COLEMAN M. L. (1985). - Geochemistry of non silicate minerals: kinetic
756 considerations. - *Philosophical Transaction of the Royal Society of London*, **315**, 39-
757 56.

758 CRAGG B. A., LAW K.M., CRAMP A, & PARKES R.J. (1998). - The response of
759 bacterial populations to sapropels in deep sediments of the Eastern Mediterranean
760 (site 969). – *In:* A.H.F Robertson, K.-C. Emeis, C. Richter, & A. Camerlenghi Eds.,
761 Proceedings of the Ocean Drilling Program, Scientific Results, Vol. 160, Texas A&M
762 University, College Station, TX, 303-307.

763 CRAMP A. & O'SULLIVAN G. (1999). - Neogene sapropels in the Mediterranean: a
764 review. - *Mar. Geol.,* **153**, 11–28.

765 DEKOV V.M., KOMY Z., ARAUJO F., VAN PUT A. & VAN GRIEKEN R. (1997). –
766 Chemical composition of sediments, suspended matter, river water and ground water
767 of the Nile (Aswan-Sohag traverse). – *The science of the total environment*, **201**,
768 195-210.

769 DEMAISON G.J. & MOORE G.T. (1980). - Anoxic environments and oil bed genesis.
770 -*Am. Assoc. Pet. Geol. Bull.*, **64**, 1179–1209.

771 DOLFING J. (2003). - Thermodynamic Considerations for Dehalogenation. – *In*: M.
772 M. Häggblom, I. D. Bossert Eds, Dehalogenation: Microbial Processes and
773 Environmental Applications. Springer, 89–114.

774 DUCASSOU E., CAPOTONDI L., MURAT A., BERNASCONI S., MULDER T.,
775 GONTHIER E., MIGEON S., DUPRAT J., GIRAUDEAU J. & MASCLE J. (2007). -

776 Multiproxy late quaternary stratigraphy of the Nile deep-sea turbidite system —
777 Towards a chronology of deep-sea terrigeneous systems. – *Sedimentary Geology,*
778 **200**, 1–13.

779 EMEIS K.C., SAKAMOTO T., WEHAUSEN R. & BRUMSACK H.J. (2000). - The
780 sapropel record of the eastern Mediterranean Sea — results of Ocean Drilling
781 Program Leg 160. - *Palaeogeogr. Palaeoclimatol. Palaeoecol*. **158**, 371–395.

782 EMERSON S. & HEDGES J.I. (1988). - Processes controlling the organic carbon
783 content of open ocean sediments. *Paleoceanography,* **3**, 621–634.

784 ESPITALIE J., LAPORTE J.L., MADEC M., MARQUIS F., LEPLAT P., PAULET J. &
785 BOUTEFEU A. (1977). - Méthode rapide de caractérisation des roches mères, de
786 leur potentiel pétrolier et de leur degré d'évolution. - *Rev. Inst. Fr. Pét*., **32**, 23–42.

787 FARMER V.C. (1974). - The Infrared Spectra of Minerals. - *Monograph, 4. The*
788 *Mineralogical Society*, London, 539 p.

789 FUTAGAMI T., MORONO Y., TERADA T., KAKSONEN A. H. & INAGAKI F. (2009). -
790 Dehalogenation activities and distribution of reductive dehalogenase homologous
791 genes in marine subsurface sediments. - *Appl. Environ. Microbiol*., **75**, 6905–6909.

792 GIESKES J.M. & MAHN C. (2007). - Halide systematics in interstitial waters of ocean
793 drilling sediment cores. - *Applied Geochemistry*, **22**, 515–533.

794 GRIBBLE G.W. (2003). - The diversity of naturally produced organohalogens.
795 *Chemosphere*, **52**, 289–297.

796 HAMANN, Y., EHRMANN, W., SCHMIEDL, G., & KUHNT, T. (2009). - Modern and
797 late Quaternary clay mineral distribution in the area of the SE Mediterranean Sea. -
798 *Quaternary Research*, **71**, 453-464.

HATCHER, P., RAVIN, A., BEHAR, F., BAUDIN, F. (2014). - Diagenesis of organic matter in a 400 m organic rich sediment core from offshore Namibia using solid state 13C NMR and FTIR. – *Org. Geochem.*, **75**, 8-23.

HARVEY G.R. (1980). - A study of the chemistry of iodine and bromine in marine sediments. - *Mar. Chem.,* **8**, 327–332.

HASSAN F.A. (1981). - Historical Nile floods and their implications for climatic change. – *Science*, **212,** 5, 1142–1144.

HATCHER P., RAVIN A., BEHAR F. & BAUDIN F. (2014). - Diagenesis of organic matter in a 400 m organic rich sediment core from offshore Namibia using solid state 13C NMR and FTIR. – *Org. Geochem.*, **75**, 8-23.

HÉBERT B., BEAUFORT D., ROY R., POURADIER A. & JIKIBAYEV R. (2015) - New methods to quantify clay minerals in the uranium deposits hosted in sands of the Chu Sarysu Basin (South Kazakhstan) based on visible and near-infrared field spectrometry. *In: Proc. 13th Biennial SGA Meeting*. - Nancy, France, 587-589.

JORISSEN F.J. (1999). - Benthic foraminiferal successions across Late Quaternary Mediterraenan sapropels. - *Mar. Geol.*, **153**, 91–101.

JUSTICIA-LEON S. D., RITALAHTI K. M., MACK E. E. & LÖFFLER F. E. (2012). - Dichloromethane fermentation by a Dehalobacter sp. in an enrichment culture derived from Pristine river sediment. - *Appl. Environ. Microbiol*., **78**, 1288–1291.

KALLEL N., DUPLESSY J.-C., LABEYRIE L., FONTUGNE M., PATERNE M. & MONTACER, M. (2000). - Mediterranean pluvial periods and sapropel formation over the last 200 000 years. - *Palaeogeogr. Palaeoclimatol. Palaeoecol.*, **157**, 45–58.

KISHK F.M., EL-ATTAR H.A., HASSAN M.N. & EL-SHEEMY H. (1976). - Mineralogical and chemical composition of the clay fraction of some Nile alluvial soils in Egypt. – *Chem. Geol.*, **17**, 295-305.

KROON D., ALEXANDER I., LITTLE, M., LOURENS L.J., MATTHEWSON A., ROBERSTON A.H.F. & SAKAMOTO T. (1998). - Oxygen isotope and sapropel stratigraphy in the eastern Mediterranean during the last 3.2 million years. – *In:* Proceedings of the Ocean Drilling Program, Scientific Results, Leg 160, 181–189.

LAWS E.A. & ARCHIE J.W. (1981). – Appropriate use of regression analysis in marine biology. - *Mar.Biol.,* **65**,13–16.

LEE M., LOW A., ZEMB O., KOENIG J., MICHAELSEN A. & MANEFIELD M. (2012). - Complete chloroform dechlorination by organochlorine respiration and fermentation. - *Environ. Microbiol*., **14**, 883–894.

LERI A. C., HAKALA J. A., MARCUS M. A., LANZIROTTI A., REDDY C.M. & MYNENI S. C. B. (2010). - Natural organobromine in marine sediments: new evidence of biogeochemical Br cycling. - *Global Biogeochem. Cycles*, **24**, GB4017.

LERI A.C., MAYER L.M., THORNTON K.R. & RAVEL B. (2014). - Bromination of marine particulate organic matter through oxidative mechanisms. – *Geochim. Cosmochim. Acta*, **142**, 53–63.

MC KINLEY J.M., WORDEN R.H. & RUFFELL A.H. (2003). Smectites in Sandstones: a review of the controls on occurrence and behaviour during diagenesis. *In:* R.H. Worden & S. Morad (Eds.), Clay mineral cements in Sandstones. Blackwell Publishing, 109-128.

MAHN, C. L. & J. M. GIESKES (2001). - Halide systematics in comparison

with nutrient distributions in sites 1033B and 1034B, Saanich Inlet: ODP Leg 169S. - *Mar. Geol*., **174**, 1‑4, 323‑339.

MALDONADO A. & STANLEY D. J. (1981). - Clay mineral distribution patterns as influenced by depositional processes in Southeastern Levantine Sea. - *Sedimentology*, **28**, 21-32.

MARTIN J. B., GIESKES J. M., TORRES M. & KASTNER M. (1993). - Bromine and iodine in Peru margin sediments and pore fluids: implications for fluid origins. *Geochim. Cosmochim. Acta*, **57**, 4377–4389.

MAYER L.M., MACKO S.A., MOOK W.H. & MURRAY S.M. (1981). – The distribution of bromine in coastal sediments and its use as a source indicator for organic matter. - *Org. Geochem.,* **3**, 37–42.

MAYER L.M. (1994). - Surface area control of organic carbon accumulation in continental shelf sediments. - *Geochim. Cosmochim. Acta*, **58**, 1271–1284.

MAYER L.M., SCHICK L.L., ALLISON M., RUTTENBERG K. & BENTLEY S. (2007). - Marine vs. terrigenous organic matter in Louisiana coastal sediments: the uses of Bromine: organic carbon ratios. - *Mar. Chem.*, **107**, 244–254.

MEYERS P.A. (2006). - Paleoceanographic and paleoclimatic similarities between Mediterranean sapropels and Cretaceous black shales. - *Palaeogeogr. Palaeoclimatol. Palaeoecol.,* **235**, 305–320.

MIDDELBURG J.J. (1989). - A simple rate model for organic-matter decomposition in marine-sediments. - *Geochim. Cosmochim. Acta*, **53**, 1577–1581.

865 MURAT A. & GOT H. (2000). - Organic carbon variations of the eastern
866 Mediterranean Holocene sapropel: a key for understanding formation processes. -
867 *Palaeogeogr. Palaeoclimatol. Palaeoecol*., **158**, 241–257.

868 OLAUSSON E. (1961). - Studies of deep-sea cores. - *Reports of the Swedish Deep*
869 *Sea Expedition 1947–1948*, **8**, 353–391.

870 ORCUTT B. N., SYLVAN J. B., KNAB N. J. & EDWARDS K. J. (2011). - Microbial
871 ecology of the dark ocean above, at, and below the seafloor. - *Microbiol. Mol. Biol.*
872 *Rev.*, **75**, 361–422.

873 PAILLARD D., LABEYRIE L. & YIOU P. (1996). - Macintosh Program performs time-
874 series analysis. – *Eos,* Trans. Am. Geophys.Union, **77**, 39, 379–379.

875 PARKES R.J., CRAGG B., ROUSSEL E., WEBSTER G., WEIGHTMAN A. & SASS
876 H. (2014). – A review of prokaryotic populations and processes in sub-seafloor
877 sediments, including biosphere: geosphere interactions. - *Mar. Geol*., **352**, 409-425.

878 PEDERSEN T. & PRICE N. (1980). - The geochemistry of iodine and bromine in
879 sediments of the Panama Basin. - *J. Mar. Res.,* **38**, 397–411.

880 PETIT S., CAILLAUD J., RIGHI, D. & MADEJOVÁ J. (2002). - Characterization and
881 crystal chemistry of an Fer-rich montmorillonite from Ölberg, Germany. - *Clay*
882 *Minerals,* **37**, 2, 283-297.

883 PETIT S. & DECARREAU A. (1990). - Hydrothermal (200 degrees C) synthesis and
884 crystal chemistry of iron-rich kaolinites. - *Clay Minerals*, **25**, 2, 141-160.

885 PRICE N. B., CALVERT S. E. & JONES P. G. W. (1970). - The distribution of iodine
886 and bromine in the sediments of the South Western Barents Sea. - *Mar. Res.***, 28,** 22-
887 34.

888 PRICE N. B. & CALVERT S. (1977). - The contrasting geochemical behaviours of
889 iodine and bromine in recent sediments from the Namibian shelf. - *Geochim.*
890 *Cosmochim. Acta*, **41**, 1769-1775.

891 PRYOR W. A. (1975). - Biogenic sedimentation and alternation of argillaceous
892 sediments in shallow marine environments. - *Geological Society of America Bulletin*,
893 **86**, 1244-1254.

894 R DEVELOPMENT CORE TEAM. (2013). - R: a Language and Environment for
895 Statistical Computing. 3-900051-07-0 *R Foundation for Statistical Computing*,
896 Vienna, Austria, URL ⟨http://www.R-project.org/⟩.

897 RICHTER T.O., VAN DER GAAST S., KOSTER B., VAARS A., GIELES R., DE
898 STIGTER H.C., DE HAAS H. & VAN WEERING T.C.E. (2006). - The Avaatech XRF
899 Core Scanner: technical description and applications to NE Atlantic sediments. -
900 *Geological Society London, Special Publication*, **267**, 39-50.

901 RICKER W.E. (1973). – Linear regressions in fishery research. - *J. De. l'Off. Des.*
902 *Rech. sur Les. Pêcheries Du. Can.,* **30**, 3,409–434.

903 ROHLING E.J. (1994). - Review and new aspects concerning the formation of
904 Mediterranean sapropels. - *Mar. Geol.,* **122**, 1–28.

905 ROHLING E.J., MARINOA G. & GRANT K.M. (2015). - Mediterranean climate and
906 oceanography, and the periodic development of anoxic events (sapropels). - *Earth-*
907 *Science Reviews*, **143**, 62–97.

908 ROSSIGNOL-STRICK M. (1985). - Mediterranean Quaternary sapropels, an
909 immediate response of the African monsoon to variations of insolation. -
910 *Palaeogeogr. Palaeoclimatol. Palaeoecol*., **49**, 237–263.

911 SCHILMAN B., ALMOGI-LABIN A., BAR-MATTHEWS M., LABEYRIE, L., PETERNE
912 M. & LUZ, B. (2001). - Long- and short-term carbon fluctuations in the eastern
913 Mediterranean during the late Holocene. – *Geology*, **29**, 12, 1099–1102.

914 SOKAL R.R. & ROHLF F.J. (2012). - Biometry: The Principles and Practice of
915 Statistics. – *in:* W. H. Freeman and Co Eds, Biological Research*,* 4th edition*.,* New
916 York*,* 937p.

917 STANLEY, D. J., NIR, Y., & GALILI, E. (1998). - Clay mineral distributions to interpret
918 Nile cell provenance and dispersal: III. Offshore margin between Nile delta and
919 northern Israel. - *Journal of coastal Research*, **14**, 196-217.

920 STEFANELLI S., CAPOTONDI L. & CIARANFI N. (2005). – Foraminiferal record and
921 environmental changes during the deposition of the Early-Middle Pleistocene
922 sapropels in southern Italy. – *Palaeogeogr. Palaeoclimatol. Palaeoecol*., **216**, 27-52.

923 SURDAM R. C., DUNN T. L., HEATHER H.P. & MACGOWAN, D.B. (1989). -
924 Integrated diagenetic modelling; a process orientated approach for clastic systems.
925 *Annual Reviews of Earth and Planetary Science Letters*, **15**, 141-170.

926 TENHAVEN H. L., DELEEUW J. W., SCHENCK P. A. & KLAVER G. T. (1988). -
927 Geochemistry of Mediterranean sediments—Bromine/organic carbon and
928 uranium/organic carbon ratios as indicators for different sources of input
929 and post-depositional oxidation, respectively. - *Org. Geochem*., **13**, 1–3,
930 255–261.

931 TJALLINGII R., RÖHL U., KÖLLING M. & BICKERT T. (2007). - Influence of the
932 water content on X-ray fluorescence core-scanning measurements in soft marine
933 sediments. - *Geochem. Geophys. Geosyst*., **8**, Q02004.

934 TISSOT B.P. & WELTE D.H. (1984). - Petroleum Formation and Occurrence. -
935 2nd. ed. Springer, Heidelberg, 601 p.

936 TRIBOVILLARD N., BOUT-ROUMAZEILLES V., SIONNEAU T., MONTERO-
937 SERRANO J.C., RIBOULLEAU A. & BAUDIN F. (2009). - Organic-matter
938 preservation and accumulation in an anoxic setting: the Orca Basin, Gulf of Mexico.
939 *Comptes Rendus Geosciences*, **341**, 1-9.

940 UPSTILL-GODDARD R. C. & ELDERFIELD H. (1988). - The role of diagenesis in the
941 estuarine budgets of iodine and bromine. - *Cont. Shelf Res.,* **8**, 405–430.

942 VETÖ I., HETÉNYI M., DEMÉNY A. & HERTELENDI E. (1994). - Hydrogen index as
943 reflecting intensity of sulphidic diagenesis in non-bioturbated, shaly sediments. – *Org.*
944 *Geochem.,* **22**, 299–310.

945 WANG P. X., TIAN J. & LOURENS L. J. (2010). - Obscuring of long eccentricity
946 cyclicity in Pleistocene oceanic carbon isotope records. - *Earth and Planetary*
947 *Science Letters*, **290**, 3-4, 319-330.

948 WORDEN R.H. & BURLEY S.D. (2003). - Sandstone diagenesis: the evolution from
949 sand to stone. - *In:* S.D. Burley & R.H. Worden (Eds.), Clastic Diagenesis: Recent
950 and Ancient, International Association of Sedimentologists, **4**, 3–44.

951 WORDEN R. H. & MORAD S. (2003). - Clay minerals in sandstones: controls on
952 formation, distribution and evolution. - *In:* R.H. Worden & S. Morad (Eds.), Clay
953 mineral cements in Sandstones. Blackwell Publishing, 3-41.

954 ZIEGLER M., JILBERT T., DE LANGE G. J., LOURENS L. J. & REICHART G.-J.
955 (2008). - Bromine counts from XRF scanning as an estimate of the marine organic
956 carbon content of sediment cores. - *G-cubed*, **9**, Q05009.

957

958 Figure captions

959 Figure 1: Morphobathymetric map of the Nile margin and location of the studied core
960 MD04 2723.

961 Figure 2: Core MD04 2723 data evolution with age: lithology, isotopic stratigraphy,
962 Marine Isotopic Stages (MIS), Ca, BrTot, TOC and Sm%.

963 Figure 3: Modified van Krevelen diagram showing the sapropel results (N=20) with
964 indications of the sapropel number and TOC content in %.

965 Figure 4: The relationship between TOC and solid-phase bromine. Bromine data
966 values below the detection limit (5 ppm) were nullifying. Black dots: S5 sequence,
967 Black squares: S28 sequence, Black dash: other sequences.

968 Figure 5: Evolution of the BrOrg/TOC ratio with age by sapropelic sequence.

969 Time is obviously a factor in BrOrg variability. The evolution of the slope (or ratio of
970 BrOrg to TOC) with age indicates a loss of BrOrg of approximately 50% in 1.1 million
971 years.

972 Figure 6: Evolution of BrOrg with age by TOC range. Red crosses: <0.5%, purple
973 dots: 1.5-2.3%, blue triangles: 2.3-3% and green squares: 4.0-6.5%.

974 Figure 7: XRD patterns of the clay material extracted from sample MD04 2723 – 1 –
975 48. Diffractograms of the oriented preparations of the less than 2 µm fraction size
976 acquired in air-dried conditions (A.D.) and after saturation with ethylene glycol.
977

978 Figure 8: Aspect of the smectitic material in the middle part of the S5 sapropelic
979 horizon (section 6, 22.5-23.5 cm): (a) SEM observation, an intimate mixture of clay
980 and carbonaceous particles in the bulk material; (b) flakes of smectite particles

deposited onto a glass slide; (c) HRTEM image of the individual crystallites of the smectite tactoids.

Figure 9: Decomposition of the near-infrared spectra of samples in which the clay material is composed of (a) 75% smectite–25% kaolinite and (b) 90% smectite–10% kaolinite. See Herbert et al., 2015 for more details on the method of quantification of Sm%.

Figure 10: Main results through time, solid-phase organic bromine evolution as a function of the TOC range (each straight line corresponds to a different debromination rate), and relative stability of the detrital montmorillonite supply.

992 Figures

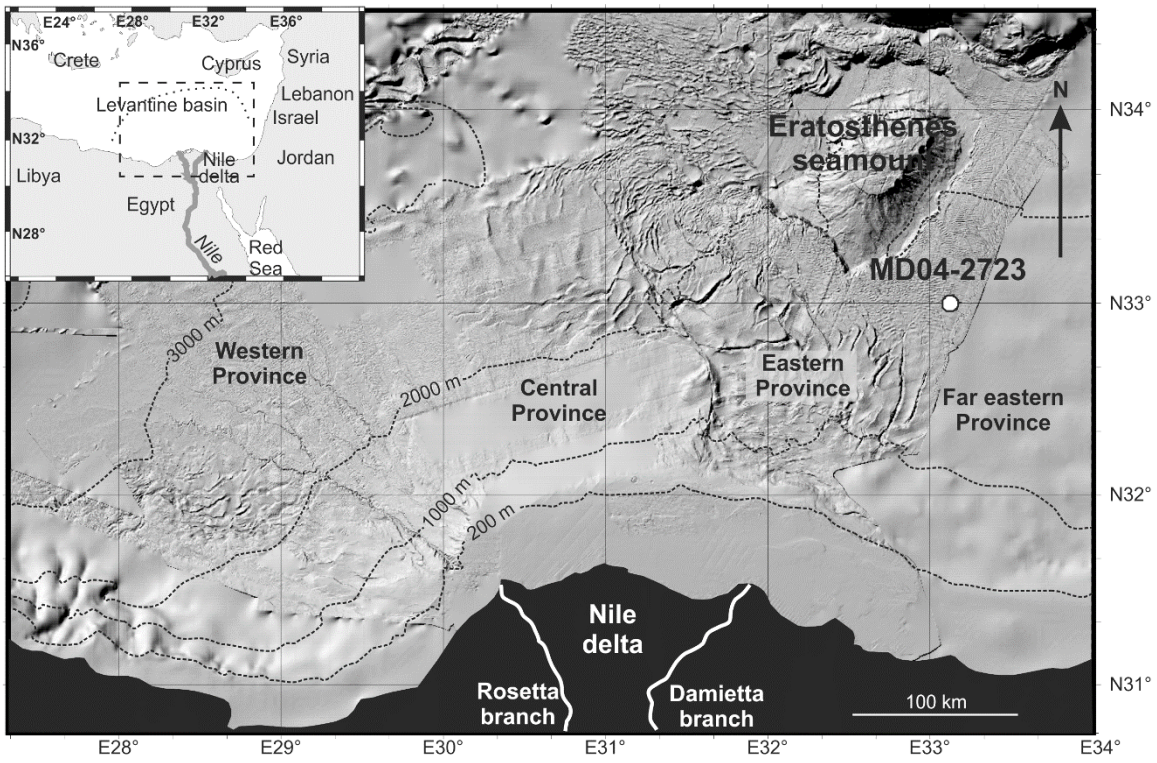

993

994 Figure 1

995

996

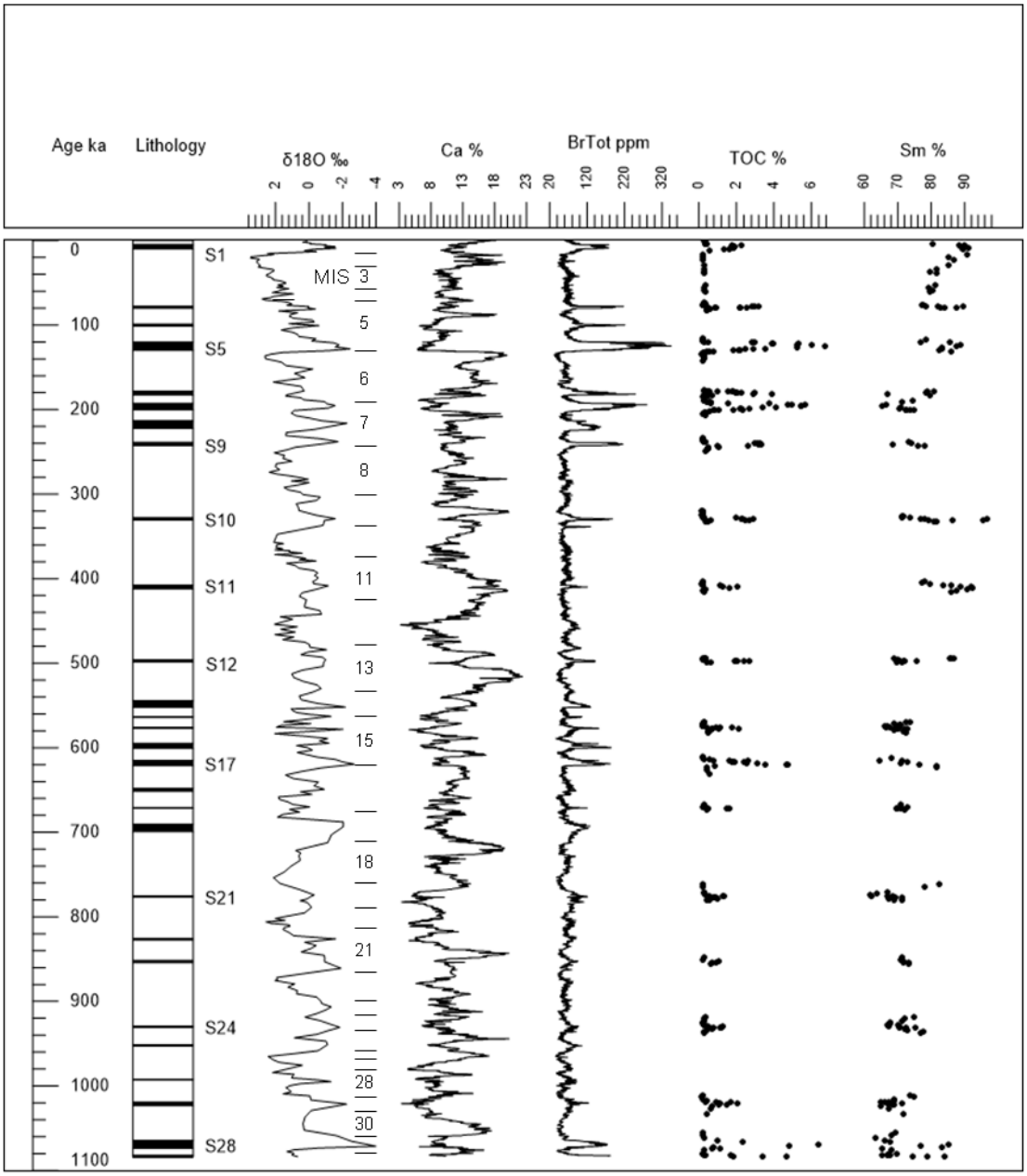

997
998 Figure 2

999

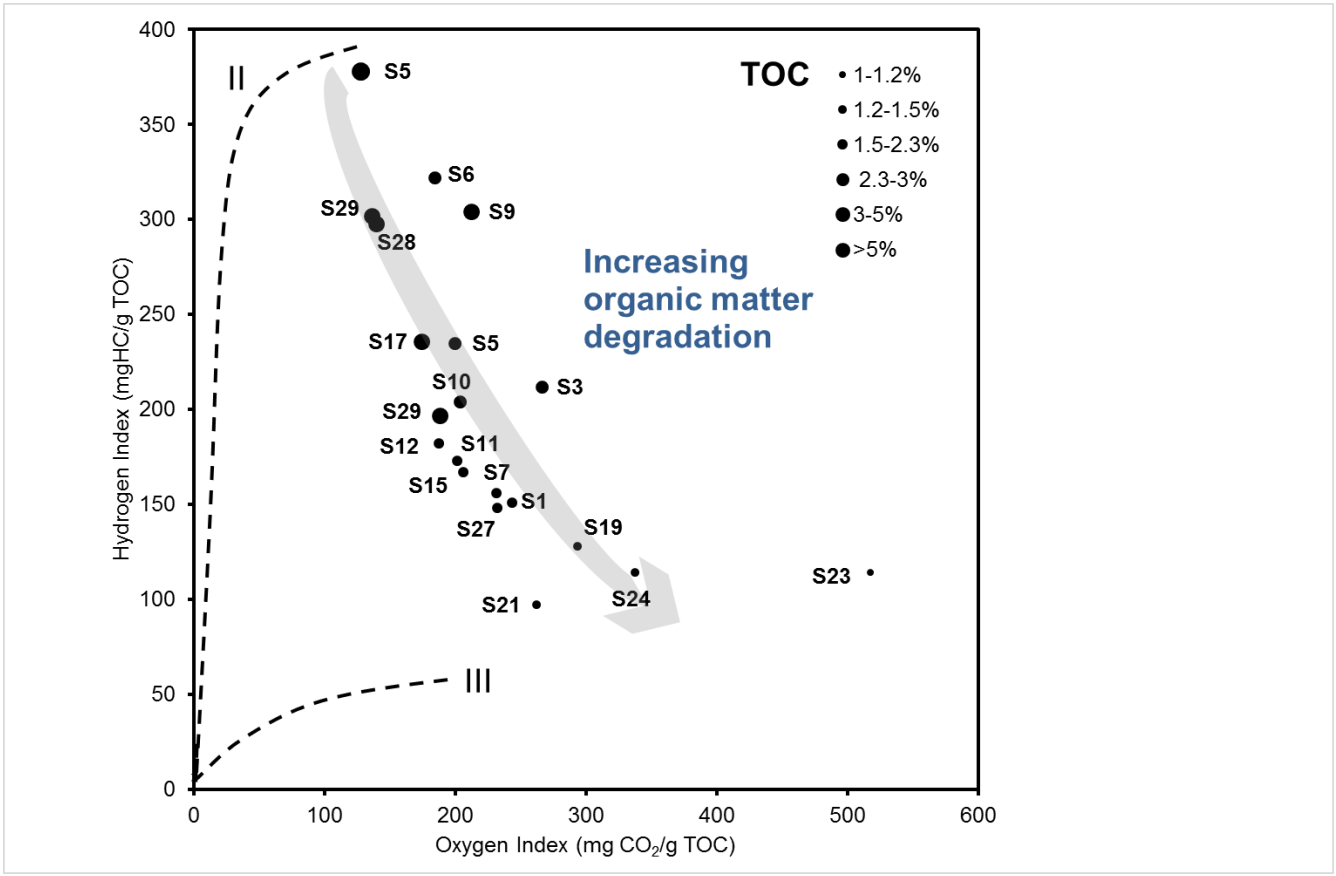
Hydrogen Index (mgHC/g TOC)
Oxygen Index (mg CO2/g TOC)
0
50
100
150
200
250
300
350
400
0
100
200
300
400
500
600
II
III
S5
S6
S29
S9
S28
S17
S5
S10
S3
S29
S12
S11
S7
S15
S1
S27
S19
S23
S21
S24
TOC
1-1.2%
1.2-1.5%
1.5-2.3%
2.3-3%
3-5%
>5%
Increasing
organic matter
degradation

Figure 3

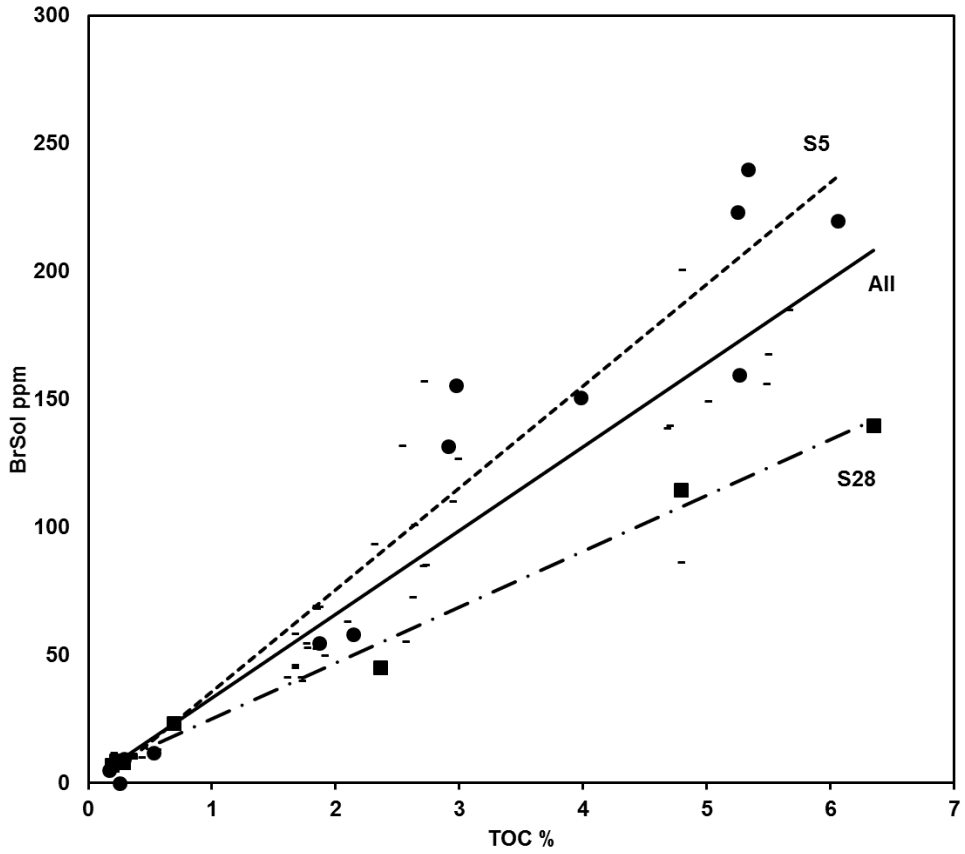

1003

1004 Figure 4

1005

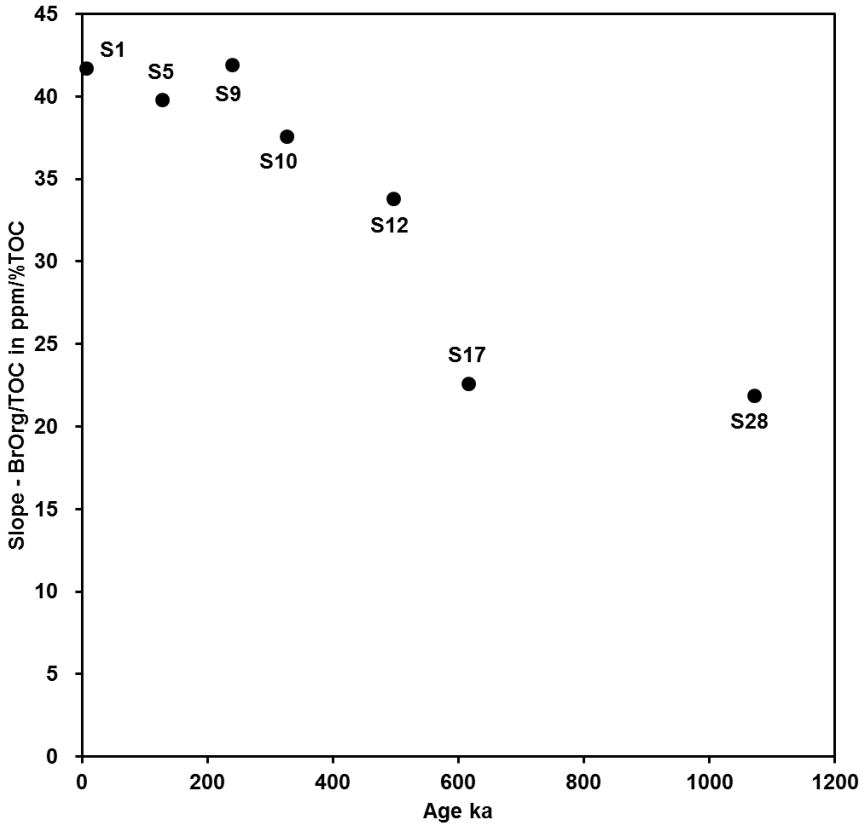

1006

1007 Figure 5

1008

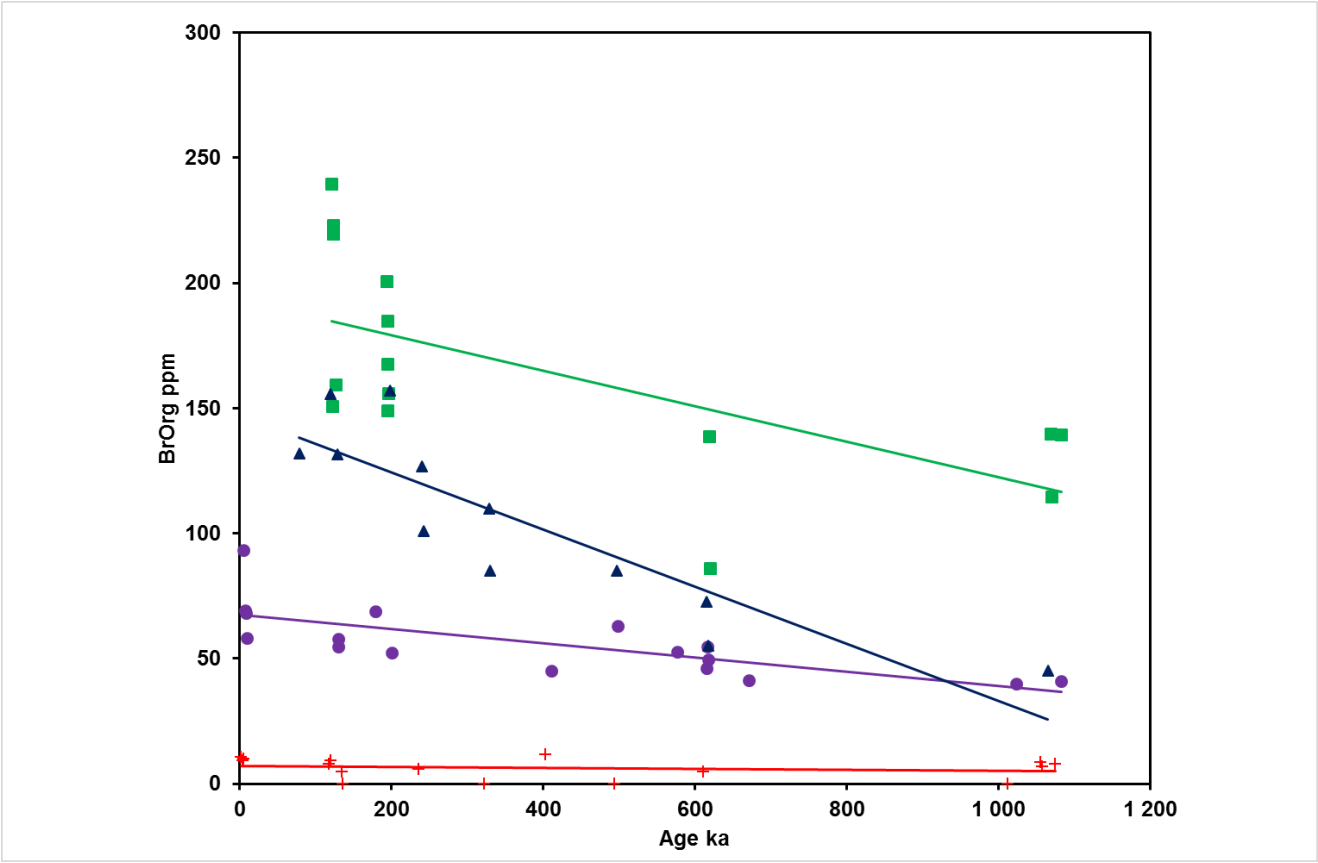

1009

1010 Figure 6

1011

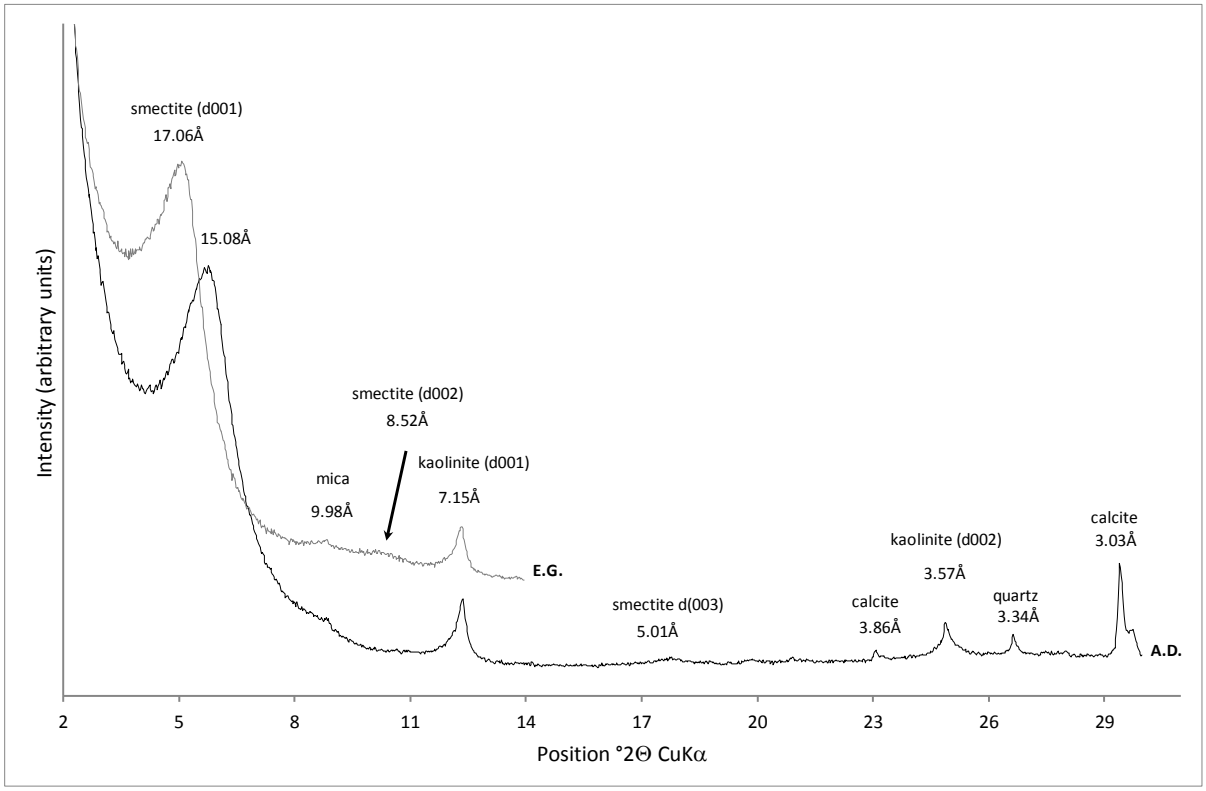

1012

1013 Figure 7

1014

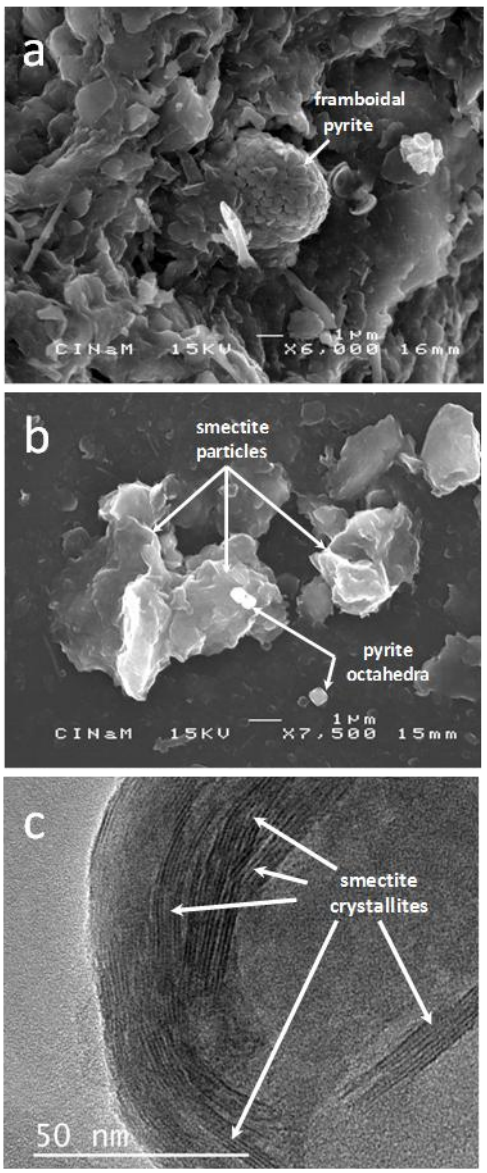

1015

1016 Figure 8

1017

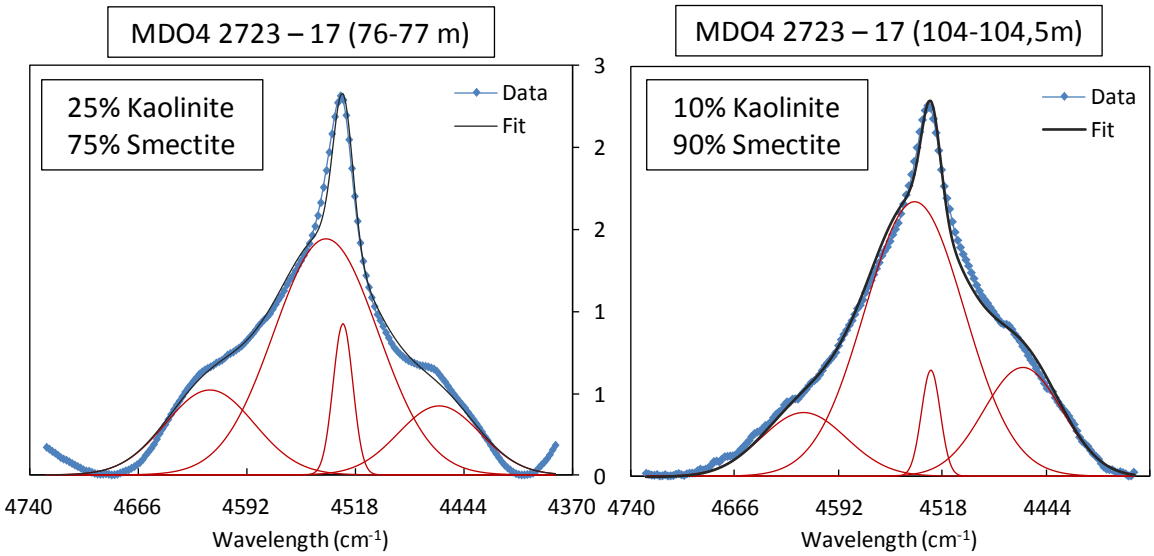

1018

1019 Figure 9

1020

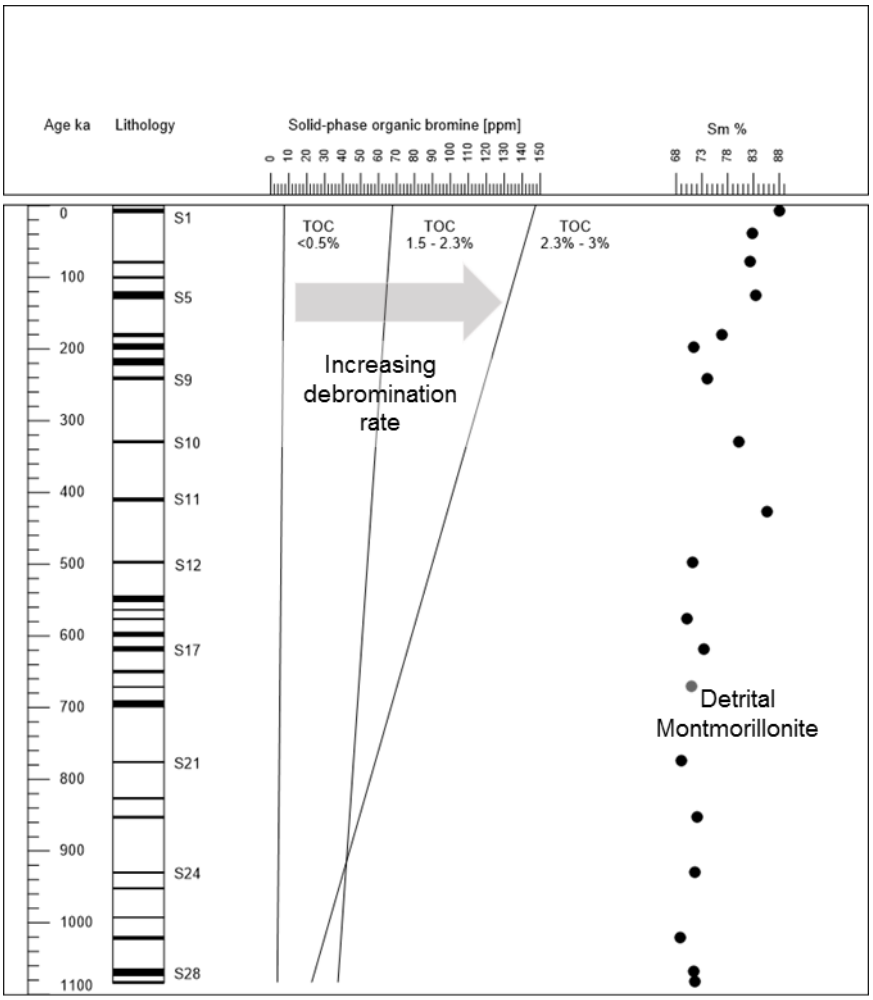

1021

1022 Figure 10

1023

Table captions

Table 1: Statistical results of the regression analysis of the TOC-BrOrg relationship. p>0.05 is non significant (NS), p between 0.05 and 0.01 is significant (S), p between 0.01 and 0.001 is highly significant (HS), and p<0.001 is very highly significant (VHS). The slope corresponds to the ratio of BrOrg to TOC in ppm/%TOC.

Table 2: Evolution of BrOrg with age by TOC range. Statistical results: p>0.05 is non significant (NS), p between 0.05 and 0.01 is significant (S), p between 0.01 and 0.001 is highly significant (HS), and p<0.001 is very highly significant (VHS).

Table 3: Representative structural formulas of smectite particles analyzed by TEM-EDX (1 and 2) and SEM-EDX(3-5). Number of ions calculated on the basis of 11 oxygens (Fe arbitrarily considered as Fe^{3+}). Int. ch: interlayer charge.

1036 Tables

Sequence	Age [ka]	N	r	r^2	*p* -value	Slope	Intercept
All data		63	0.922	0.851	VHS	32.8	0.44
S1	6.13	8	0.996	0.993	VHS	41.7	-6.83
S5	127.47	14	0.968	0.937	VHS	39.8	-3.90
S9	238.94	3	0.996	0.992	NS	41.9	-2.72
S10	326.65	3	0.991	0.982	NS	37.6	-7.51
S12	495.89	3	0.999	0.999	S	33.8	-6.86
S17	615.48	8	0.909	0.825	HS	22.6	7.06
S28	1071.57	7	0.995	0.990	VHS	21.9	3.13

1037

1038 Table 1

1039

TOC range	Mean TOC	N	r	r^2	*p* -value	Slope	Intercept	% of loss BrOrg in 1 m.y.	Debromination rate [µmolBrOrg $molC^{-1}$ y^{-1}]
< 0.5%	0.24	16	-0.171	0.029	NS	-0.002	6.92	NS	NS
1.5 - 2.3 %	1.83	17	-0.736	0.542	HS	-0.028	67.53	41	$2.3\ 10^{-4}$
2.3 - 3.0 %	2.73	12	-0.878	0.771	HS	-0.115	147.46	78	$6.3\ 10^{-4}$
4.55 - 5.4%	4.95	9	-0.688	0.473	S	-0.087	201.34	43	$2.6\ 10^{-4}$
5.4 - 6.5%	5.80	5	-0.671	0.450	NS	-0.051	192.07	NS	NS
4.0 - 6.5 %	5.17	15	-0.640	0.410	S	-0.071	193.31	37	$2.0\ 10^{-4}$

Table 2

	1	2	3	4	5
Si	3.97	3.83	3.91	3.91	3.84
Al^{IV}	0.03	0.17	0.09	0.09	0.16
Al^{VI}	1.24	1.14	1.35	0.88	1.45
Fe^{3+}	0.31	0.26	0.28	0.53	0.26
Mg	0.53	0.65	0.37	0.59	0.29
Ca	0.09	0.17	0.03	0.05	0.14
Na	0.10	0.17	0.25	0.31	0.12
K	0.06	0.14	0.14	0.26	0.07
Int. Ch.	0.35	0.65	0.45	0.67	0.47

1043

1044 Table 3